Publications of the Astronomical Society of the Pacific, 138:084101 (25pp), 2026 August https://doi.org/10.1088/1538-3873/ae8a7e

Constraints on the VHE Counterpart of Two Binary Black Hole Mergers Observed by the MAGIC and CTAO LST-1 Telescopes

K. Abe[1], S. Abe[2], J. Abhir[3], A. Abhishek[4], V. A. Acciari[5], F. Acero[6,7], A. Aguasca-Cabot[8], I. Agudo[9], I. Albanese[10], D. Ambrosino[11], F. Ambrosino[12], T. Aniello[12], S. Ansoldi[13,14], L. A. Antonelli[12], C. Aramo[11], C. Arauner[15], A. Arbet-Engels[16], C. Arcaro[10], T.T.H. Arnesen[17], P. Aubert[18], A. Babić[19], C. Bakshi[20], A. Baktash[21], M. Balbo[22], A. Bamba[23], A. Baquero Larriva[24,25], U. Barres de Almeida[26], J. A. Barrio[24], L. Barrios Jiménez[17], I. Batkovic[10], J. Baxter[2], J. Becerra González[17,27], W. Bednarek[28], E. Bernardini[10], J. Bernete[29], A. Berti[16], J. Besenrieder[16], C. Bigongiari[12], A. Biland[3], E. Bissaldi[30], O. Blanch[5], Ž. Bošnjak[19], G. Bonnoli[31], P. Bordas[8], L. Breton-Zaourat[18], A. Briscioli[32], E. Bronzini[33], G. Brunelli[34], J. Buces[24], A. Bulgarelli[34], I. Burelli[5], L. Burmistrov[22], C. Campa[33], A. Campoy-Ordaz[35], M. Cardillo[36], S. Caroff[18], A. Carosi[12], R. Carosi[37], R. Carraro[12], M. Carretero-Castrillo[8], F. Cassol[32], A. J. Castro-Tirado[9], D. Cerasole[38], G. Ceribella[16], A. Cerviño Cortínez[24], Y. Chai[2,16], A. Chiavassa[39,40], A. Chilingarian[41], G. Chon[16], L. Chytka[42], G. M. Cicciari[43,44], A. Cifuentes Santos[29], J. L. Contreras[24], J. Cortina[29], H. Costantini[32], S. Covino[31,45], M. Croisonnier[5], G. D'Amico[5], P. Da Vela[34], M. Dalchenko[22], F. Dazzi[33], A. De Angelis[10], M. de Bony de Lavergne[32], B. De Lotto[13], R. de Menezes[26], G. De Palma[30], V. de Souza[46], R. Del Burgo[11], L. Del Peral[47], M. Delfino[5,48], C. Delgado Mendez[29], J. Delgado Mengual[5,48], D. della Volpe[22], L. Di Bella[15], C. Di Domenico[49], A. Di Piano[34], F. Di Pierro[39], R. Di Tria[38], L. Di Venere[50], C. Díaz[29], A. Dinesh[24], E. Do Souto Espiñeira[29], D. Dominis Prester[51], A. Donini[12], D. Dorner[52], M. Doro[10], L. Eisenberger[52], D. Elsässer[15], G. Emery[9], J. Escudero[9], L. Fariña[5], L. Feligioni[32], F. Ferrarotto[53], A. Fiasson[18,54], L. Foffano[36], L. Font[35], F. Frías García-Lago[17], Y. Fukazawa[55], S. Gallozzi[12], J. Garcia Garcia[9], R. J. García López[17], S. Garcia Soto[29], D. Gasparrini[49], S. Gasparyan[56], M. Gaug[35], J. G. Giesbrecht Paiva[26], N. Giglietto[30], F. Giordano[38], P. Gliwny[28], N. Godinovic[57], T. Gradetzke[15], R. Grau[2], J. Green[16], G. Grolleron[18], S. Gunji[58], P. Günther[52], D. Hadasch[59], A. Hahn[16], M. Hashizume[55], T. Hassan[29], K. Hayashi[2,60], L. Heckmann[16,61], M. Heller[22], J. Herrera Llorente[17], N. Hiroshima[2], D. Hoffmann[32], D. Horns[21], J. Houles[32], D. Hrupec[62], T. Inada[2], S. Inoue[2,63], K. Ioka[64], M. Iori[53], D. Israyelyan[56], A. Iuliano[11], J. Jahanvi[13], I. Jiménez Martínez[16], J. Jiménez Quiles[5,101], I. Jorge Rodrigo[29], J. Jurysek[65], M. Kagaya[2,60], S. Kankkunen[66], V. Karas[67], H. Katagiri[68], T. Kayanoki[55], D. Kerszberg[5,69], M. Khachatryan[56], G. W. Kluge[70,71], Y. Kobayashi[2], K. Kohri[72], J. Konrad[15], P. Kornecki[9], P. M. Kouch[66], H. Kubo[2], J. Kushida[1], B. Lacave[22], M. Láinez[24], A. Lamastra[12], L. Lemoigne[18], E. Lindfors[66], M. Linhoff[15], S. Lombardi[12], F. Longo[73], R. López-Coto[9], M. López-Moya[24], A. López-Oramas[17], S. Loporchio[38], A. Lorini[4], J. Lozano Bahilo[47], F. Lucarelli[12], H. Luciani[73], L. Lulić[51], P. L. Luque-Escamilla[74], P. Majumdar[2,20], M. Makariev[75], M. Mallamaci[43,44], D. Mandat[65], G. Maneva[75], M. Manganaro[51], S. Mangano[29], D. K. Maniadakis[76], G. Manicò[44], K. Mannheim[52], F. Marini[10], M. Mariotti[10], G. Marsella[43,44], J. Martí[74], D. Martin[24], G. Martínez[29], M. Martínez[5], O. Martinez[77,78], P. Maruševec[19], M. Massa[4], D. Mazin[2], S. Menchiari[9], J. Méndez-Gallego[9], S. Menon[12,79], E. Mestre Guillen[59], D. Miceli[10], T. Miener[22], J. M. Miranda[78], J. M. Miranda[4], R. Mirzoyan[16], M. Mizuno[55], M. Molero Gonzalez[29], E. Molina[17], H. A. Mondal[2], T. Montaruli[22], A. Moralejo[5], S. Morales Sanchez De Lozada[73], K. Morita[2], A. Morselli[49], V. Moya[24], K. Mrakovcic[51], A. L. Müller[65], H. Muraishi[80], T. Nagata[2], S. Nagataki[81], T. Nakamori[58], C. Nanci[34], A. Negro[82], A. Neronov[83], V. Neustroev[84], D. Nieto Castaño[24], M. Nievas Rosillo[17], C. Nigro[5], L. Nikolić[4], K. Nilsson[66], K. Noda[2,63], V. Novotny[85], S. Nozaki[2], M. Ohishi[2], A. Okumura[86,87], R. Orito[88], L. Orsini[89], J. Otero- Santos[10], P. Ottanelli[89], S. Paiano[76], M. Palatiello[12], G. Panebianco[34], D. Paneque[16], R. Paoletti[4], J. M. Paredes[8], M. Pech[42,65], M. Pecimotika[62,90,101], M. Peresano[16], F. Perrotta[91], M. Persic[13,92], F. Pfeifle[52], E. Pietropaolo[93], M. Pihet[9], G. Pirola[16], C. Plard[18], F. Podobnik[4], M. Polo[29], C. Pozo-Gonzaléz[9], P. G. Prada Moroni[37], E. Prandini[10], S. Rainò[38], R. Rando[10], W. Rhode[15], M. Ribó[8], J. Rico[5], V. Rizi[93], G. Rodriguez Fernandez[49], A. Roy[55], E. Ruiz-Velasco[18], N. Sahakyan[56], T. Saito[2], S. Sakurai[2], D. A. Sanchez[18], H. Sano[2,94], E. Santos Moura[46], T. Šaric[57], Y. Sato[95], F. G. Saturni[12], V. Savchenko[83], F. Schiavone[38], K. Schmitz[15], F. Schussler[96], T. Schweizer[16], M. Seglar Arroyo[5,101], U. Sharma[5], T. Siegert[52], G. Silvestri[10], A. Simongini[12,79,101], J. Sitarek[28], V. Sliusar[97], D. Sobczynska[28], I. Sofia[39], A. Stamerra[12], J. Striškovic[62], D. Strom[16], M. Strzys[2], Y. Suda[55], A. Sunny[12,79], H. Tajima[86], M. Takahashi[86], R. Takeishi[2], S. J. Tanaka[95], J. Tartera Barberà[5], T. Tavernier[65], P. Temnikov[75], Y. Terada[98], K. Terauchi[99], T. Terzic[51], M. Teshima[2,16], M. Tluczykont[21], T. Tomura[2], D. F. Torres[59], F. Tramonti[4], P. Travnicek[65], G. Tripodo[44], A. Tutone[76], S. Ubach[35],

M. Vacula[42], M. Vázquez Acosta[17], S. Ventura[4], G. Verna[4], I. Viale[82], A. Viana[46], A. Vigliano[13], C. F. Vigorito[39,40], E. Visentin[39,40], V. Vitale[49], M. Vorbrugg[52], G. Voutsinas[22], I. Vovk[2], T. Vuillaume[18], R. Walter[97], C. Walther[15], L. Wan[2], P. Witczak[28], F. Wersig[15], T. Yamamoto[100], R. Yamazaki[95], Y. Yao[1], P. K. H. Yeung[2], T. Yoshida[68], T. Yoshikoshi[2], and W. Zhang[59]

(The MAGIC and CTAO-LST Collaborations)

[1] Department of Physics, Tokai University, 4-1-1, Kita-Kaname, Hiratsuka, Kanagawa 259-1292, Japan

[2] Institute for Cosmic Ray Research, University of Tokyo, 5-1-5, Kashiwa-no-ha, Kashiwa, Chiba 277-8582, Japan

[3] ETH Zürich, CH-8093 Zürich, Switzerland

[4] INFN and Universit'a degli Studi di Siena, Dipartimento di Scienze Fisiche, della Terra e dell'Ambiente (DSFTA), Sezione di Fisica, Via Roma 56, 53100 Siena, Italy

[5] Institut de Fisica d'Altes Energies (IFAE), The Barcelona Institute of Science and Technology, Campus UAB, 08193, Bellaterra (Barcelona), Spain

[6] Université Paris-Saclay, Université Paris Cité, CEA, CNRS, AIM, F-91191 Gif-sur-Yvette Cedex, France

[7] FSLAC IRL 2009, CNRS/IAC, La Laguna, Tenerife, Spain

[8] Departament de Física Quàntica i Astrofísica, Institut de Ciències del Cosmos, Universitat de Barcelona, IEEC-UB, Martí i Franquès, 1, 08028, Barcelona, Spain

[9] Instituto de Astrofísica de Andalucía-CSIC, Glorieta de la Astronomía s/n, 18008, Granada, Spain

[10] INFN Sezione di Padova and Università degli Studi di Padova, Via Marzolo 8, 35131 Padova, Italy

[11] INFN Sezione di Napoli, Via Cintia, ed. G, 80126 Napoli, Italy

[12] INAF - Osservatorio Astronomico di Roma, Via di Frascati 33, 00040, Monteporzio Catone, Italy

[13] INFN Sezione di Trieste and Università degli studi di Udine, via delle scienze 206, 33100 Udine, Italy

[14] also at International Center for Relativistic Astrophysics (ICRA), Rome, Italy

[15] Department of Physics, TU Dortmund University, Otto-Hahn-Str. 4, 44227 Dortmund, Germany

[16] Max-Planck-Institut für Physik, Boltzmannstraße 8, 85748, Garching bei München, Germany

[17] Instituto de Astrofísica de Canarias and Departamento de Astrofísica, Universidad de La Laguna, C. Vía Láctea, s/n, 38205, La Laguna, Santa Cruz de Tenerife, Spain

[18] Univ. Savoie Mont Blanc, CNRS, Laboratoire d'Annecy de Physique des Particules—IN2P3, 74000 Annecy, France

[19] Croatian MAGIC Group: University of Zagreb, Faculty of Electrical Engineering and Computing (FER), 10000 Zagreb, Croatia

[20] Saha Institute of Nuclear Physics, A CI of Homi Bhabha National Institute, Kolkata 700064, West Bengal, India

[21] Universität Hamburg, Institut für Experimentalphysik, Luruper Chaussee 149, 22761 Hamburg, Germany

[22] Université de Genève, Département de Physique Nucléaire et Corpusculaire, 24 Quai Ernest Ansermet 1211 Genève 4, Switzerland

[23] Graduate School of Science, University of Tokyo, 7-3-1 Hongo, Bunkyo-ku, Tokyo 113-0033, Japan

[24] IPARCOS-UCM, Instituto de Física de Partículas y del Cosmos, and EMFTEL Department, Universidad Complutense de Madrid, Plaza de Ciencias, 1. Ciudad Universitaria, 28040 Madrid, Spain

[25] Faculty of Science and Technology, Universidad del Azuay, Cuenca, Ecuador

[26] Centro Brasileiro de Pesquisas Físicas, Rua Xavier Sigaud 150, RJ 22290-180, Rio de Janeiro, Brazil

[27] Consejo Superior de Investigaciones Científicas (CSIC), 28006, Spain

[28] Faculty of Physics and Applied Informatics, University of Lodz, ul. Pomorska 149-153, 90-236 Lodz, Poland

[29] CIEMAT, Avda. Complutense 40, 28040 Madrid, Spain

[30] INFN Sezione di Bari and Politecnico di Bari, via Orabona 4, 70124 Bari, Italy

[31] INAF - Osservatorio Astronomico di Brera, Via Brera 28, 20121 Milano, Italy

[32] Aix Marseille Univ, CNRS/IN2P3, CPPM, Marseille, France

[33] National Institute for Astrophysics (INAF), I-00136 Rome, Italy

[34] INAF - Osservatorio di Astrofisica e Scienza dello spazio di Bologna, Via Piero Gobetti 93/3, 40129 Bologna, Italy

[35] Departament de Física, and CERES-IEEC, Universitat Autònoma de Barcelona, E-08193 Bellaterra, Spain

[36] INAF—Istituto di Astrofisica e Planetologia Spaziali (IAPS), Via del Fosso del Cavaliere 100, 00133 Roma, Italy

[37] Università di Pisa and INFN Pisa, I-56126 Pisa, Italy

[38] INFN Sezione di Bari and Università di Bari, via Orabona 4, 70126 Bari, Italy

[39] INFN Sezione di Torino, Via P. Giuria 1, 10125 Torino, Italy

[40] Dipartimento di Fisica—Universitá degli Studi di Torino, Via Pietro Giuria 1—10125 Torino, Italy

[41] Armenian MAGIC Group: A. Alikhanyan National Science Laboratory, 0036 Yerevan, Armenia

[42] Palacky University Olomouc, Faculty of Science, 17. listopadu 1192/12, 771 46 Olomouc, Czechia

[43] Dipartimento di Fisica e Chimica "E. Segrè" Università degli Studi di Palermo, via delle Scienze, 90128 Palermo, Italy

[44] INFN Sezione di Catania, Via S. Sofia 64, 95123 Catania, Italy

[45] Also at Como Lake centre for AstroPhysics (CLAP), DiSAT, Università dell'Insubria, via Valleggio 11, 22100 Como, Italy

[46] Instituto de Física de Sao Carlos, Universidade de Sao Paulo, Av. Trabalhador Sao-carlense, 400—CEP 13566-590, Sao Carlos, SP, Brazil

[47] University of Alcalá UAH, Departamento de Physics and Mathematics, Pza. San Diego, 28801, Alcalá de Henares, Madrid, Spain

[48] also at Port d'Informació Científica (PIC), E-08193 Bellaterra (Barcelona), Spain

[49] INFN Sezione di Roma Tor Vergata, Via della Ricerca Scientifica 1, 00133 Rome, Italy

[50] INFN Sezione di Bari, via Orabona 4, 70125, Bari, Italy

[51] University of Rijeka, Faculty of Physics, Radmile Matejcic 2, 51000 Rijeka, Croatia

[52] Institute for Theoretical Physics and Astrophysics, Universität Würzburg, Campus Hubland Nord, Emil-Fischer-Str. 31, 97074, Würzburg, Germany

[53] INFN Sezione di Roma La Sapienza, P.le Aldo Moro, 2—00185 Rome, Italy

[54] ILANCE, CNRS—University of Tokyo International Research Laboratory, University of Tokyo, 5-1-5 Kashiwa-no-Ha Kashiwa City, Chiba 277-8582, Japan

[55] Physics Program, Graduate School of Advanced Science and Engineering, Hiroshima University, 1-3-1 Kagamiyama, Higashi-Hiroshima City, Hiroshima, 739-8526, Japan

[56] Armenian MAGIC Group: ICRANet-Armenia, 0019 Yerevan, Armenia

[57] University of Split, FESB, R. Boškovića 32, 21000 Split, Croatia

[58] Department of Physics, Yamagata University, 1-4-12 Kojirakawa-machi, Yamagata-shi, 990-8560, Japan

[59] Institute of Space Sciences (ICE, CSIC), and Institut d'Estudis Espacials de Catalunya (IEEC), and Instituci'o Catalana de Recerca I Estudis Avançats (ICREA), Campus UAB, Carrer de Can Magrans, s/n 08193 Bellatera, Spain; lst-contact@cta-observatory.org; contact.magic@mpp.mpg.de

[60] Sendai College, National Institute of Technology, 4-16-1 Ayashi-Chuo, Aoba-ku, Sendai city, Miyagi 989-3128, Japan

[61] Université Paris Cité, CNRS, Astroparticule et Cosmologie, F-75013 Paris, France
[62] Josip Juraj Strossmayer University of Osijek, Department of Physics, Trg Ljudevita Gaja 6, 31000 Osijek, Croatia
[63] Chiba University, 1-33, Yayoicho, Inage-ku, Chiba-shi, Chiba, 263-8522, Japan
[64] Kitashirakawa Oiwakecho, Sakyo Ward, Kyoto, 606-8502, Japan
[65] FZU—Institute of Physics of the Czech Academy of Sciences, Na Slovance 1999/2, 182 21 Praha 8, Czechia
[66] Finnish MAGIC Group: Finnish Centre for Astronomy with ESO, Department of Physics and Astronomy, University of Turku, FI-20014 Turku, Finland
[67] Astronomical Institute of the Czech Academy of Sciences, Bocni II 1401—14100 Prague, Czechia
[68] Faculty of Science, Ibaraki University, 2 Chome-1-1 Bunkyo, Mito, Ibaraki 310-0056, Japan
[69] Sorbonne Université, CNRS/IN2P3, Laboratoire de Physique Nucléaire et de Hautes Energies, LPNHE, 4 place Jussieu, 75005 Paris, France
[70] Also at Department of Physics, University of Oslo, Norway
[71] Department for Physics and Technology, University of Bergen, Norway
[72] Institute of Particle and Nuclear Studies, KEK (High Energy Accelerator Research Organization), 1-1 Oho, Tsukuba, 305-0801, Japan
[73] INFN Sezione di Trieste and Università degli Studi di Trieste, Via Valerio 2 I, 34127 Trieste, Italy
[74] Escuela Politécnica Superior de Jaén, Universidad de Jaén, Campus Las Lagunillas s/n, Edif. A3, 23071, Jaén, Spain
[75] Institute for Nuclear Research and Nuclear Energy, Bulgarian Academy of Sciences, 72 boul. Tsarigradsko chaussee, 1784 Sofia, Bulgaria
[76] INAF Istituto di Astrofisica Spaziale e Fisica Cosmica di Palermo, Via Ugo La Malfa 153, Palermo, I-90146, Italy
[77] Departamento de Geología, Física y Química Inorgánica, Universidad Rey Juan Carlos, C/ Tulipán s/n, 28933, Móstoles, Madrid, Spain
[78] Grupo de Electronica, Universidad Complutense de Madrid, Av. Complutense s/n, 28040 Madrid, Spain
[79] Macroarea di Scienze MMFFNN, Università di Roma Tor Vergata, Via della Ricerca Scientifica 1, 00133 Rome, Italy
[80] School of Allied Health Sciences, Kitasato University, Sagamihara, Kanagawa 228-8555, Japan
[81] RIKEN, Institute of Physical and Chemical Research, 2-1 Hirosawa, Wako, Saitama, 351-0198, Japan
[82] INFN MAGIC Group: INFN Sezione di Torino and Università degli Studi di Torino, I-10125 Torino, Italy
[83] Laboratory for High Energy Physics, École Polytechnique Fédérale, CH-1015 Lausanne, Switzerland
[84] Finnish MAGIC Group: Space Physics and Astronomy Research Unit, University of Oulu, FI-90014 Oulu, Finland
[85] Charles University, Institute of Particle and Nuclear Physics, V Holešovičk'ach 2, 180 00 Prague 8, Czechia
[86] Institute for Space-Earth Environmental Research, Nagoya University, Chikusa-ku, Nagoya 464-8601, Japan
[87] Kobayashi-Maskawa Institute (KMI) for the Origin of Particles and the Universe, Nagoya University, Chikusa-ku, Nagoya 464-8602, Japan
[88] Graduate School of Technology, Industrial and Social Sciences, Tokushima University, 2-1 Minamijosanjima, Tokushima, 770-8506, Japan
[89] INFN Sezione di Pisa, Edificio C—Polo Fibonacci, Largo Bruno Pontecorvo 3, 56127 Pisa, Italy
[90] Department of Polytechnics, Dr. Franjo Tudman Defense and Security University, Ilica 256b, 10000 Zagreb, Croatia
[91] Istituto Nazionale di Astrofisica—Osservatorio Astronomico di Capodimonte, Via Moiariello 16, 80131, Napoli, Italy
[92] Also at INAF Padova
[93] INFN Dipartimento di Scienze Fisiche e Chimiche—Università degli Studi dell'Aquila and Gran Sasso Science Institute, Via Vetoio 1, Viale Crispi 7, 67100, L'Aquila, Italy
[94] Gifu University, Faculty of Engineering, 1-1 Yanagido, Gifu 501-1193, Japan
[95] Department of Physical Sciences, Aoyama Gakuin University, Fuchinobe, Sagamihara, Kanagawa, 252-5258, Japan
[96] IRFU, CEA, Université Paris-Saclay, Bât 141, 91191, Gif-sur-Yvette, France
[97] Department of Astronomy, University of Geneva, Chemin d'Ecogia 16, CH-1290 Versoix, Switzerland
[98] Graduate School of Science and Engineering, Saitama University, 255 Simo-Ohkubo, Sakura-ku, Saitama city, Saitama 338-8570, Japan
[99] Division of Physics and Astronomy, Graduate School of Science, Kyoto University, Sakyo-ku, Kyoto, 606-8502, Japan
[100] Department of Physics, Konan University, 8-9-1 Okamoto, Higashinada-ku Kobe 658-8501, Japan
Received 2026 June 3; revised 2026 July 6; accepted 2026 July 14; published 2026 August 6

Abstract

We present very-high-energy gamma-ray observations of two binary black hole merger candidates, GW240615_113620 and GW241125_010116, performed with the Major Atmospheric Gamma Imaging Cherenkov (MAGIC) telescopes and the first Large-Sized Telescope of the Cherenkov Telescope Array Observatory's (CTAO LST-1). GW240615_113620 was the best localized event of the fourth observing run of the LIGO-Virgo-KAGRA gravitational waves interferometers. GW241125_010116 was temporally and spatially coincident with a sub-threshold short-duration burst detected with the Swift-Burst Alert Telescope, the Swift-X-Ray Telescope and the Einstein Probe Follow-up X-ray Telescope. We observed the two events in stereoscopic mode, taking advantage of the improved sensitivity of joint MAGIC+LST-1 observations. No detection was achieved in the GeV–TeV gamma-ray band for any of the two sources. The unfavourable observing conditions of both events posed a challenge for a standard analysis and therefore a non standard analysis was necessary for both objects. Owing to the small localization area and the association with a GRB-like burst respectively, these events represented an unprecedented opportunity to study in details the electromagnetic emission from binary black holes

[101] Corresponding authors.

merger events and, in particular, we discussed two theoretical models that predict a detectable gamma-ray emission and the possible future applications.

Unified Astronomy Thesaurus concepts: Gravitational waves (678); Gamma-rays (637); Transient sources (1851)

1. Introduction

The first detection of a gravitational wave (GW) from a binary black hole (BBH) system merger was a historical breakthrough, marking the beginning of multimessenger astronomy as we know it today (Abbott et al. 2016). This led to a technological advance on GW interferometers, currently the Advanced Laser Interferometer Gravitational Wave Observatory (LIGO; Aasi et al. 2015), Advanced Virgo + (Acernese et al. 2014; Flaminio 2020) and Kamioka Gravitational Wave Detector (KAGRA; Aso et al. 2013), and corresponding LIGO-Virgo-KAGRA (LVK) Collaboration(s). Improvements in broadband sensitivity led to growth in the number of candidate GW events detected throughout the first four observing runs, achieving a total of 390 confirmed events so far.[102] Among them, 11 were observed during the first two observing runs (O1 and O2; Abbott et al. 2019a), 79 during the first and second half of the third run (O3a and O3b; Abbott et al. 2021a, 2023, 2024), 139 during the first part of the fourth run (O4a; Abac et al. 2024; Abac et al. 2025), and the remaining 161 during the second part of the fourth run (04b; LVK Collaboration 2026a, 2026b). The vast majority of confirmed detections originate from BBH systems, with total masses in the range $3.4-236 M_{\odot}$, corresponding to chirp masses of 1.2–$101 M_{\odot}$ and distances up to 8.3 Gpc. Among the four observing runs, only two events were classified as binary neutron star (BNS; Abbott et al. 2017a, 2020) and three neutron-star–black hole binaries (NSBHs; Abbott et al. 2021b; Abac et al. 2024).

Detecting electromagnetic (EM) counterparts of GW events is one of the main challenges of current astrophysics and many facilities around the world and in space are dedicating their efforts to make this detection possible. The historical detection of GW170817 from a BNS merger by LIGO and Virgo (Abbott et al. 2017a, 2019, 2019b) demonstrated the importance of multimessenger astronomy (the first time being the electromagnetic and neutrino detection of SN 1987A; e.g., Hirata et al. 1988). Remarkably, the GW was spatially and timely coincident with a short gamma-ray burst (GRB), GRB 170817A, detected by the Fermi Gamma-Ray Burst Monitor (GBM; Goldstein et al. 2017) and the INTErnational Gamma-Ray Astrophysics Laboratory (INTEGRAL; Savchenko et al. 2017) space satellites, providing strong evidence of the association between BNS mergers and GRBs (Abbott et al. 2017b). Soon after the initial trigger, an extensive follow-up campaign was launched across the entire EM spectrum leading to the detection of the optical/NIR counterpart AT 2017gfo, followed by X-rays and radio detection of the GRB afterglow (Abbott et al. 2017 and references therein). The afterglow was extensively followed in the gamma-ray band, spanning over 10 orders of magnitude in energy by space and ground-based telescopes. However, no significant detection was achieved in any gamma-ray band (Goldstein et al. 2017; Kocevski et al. 2017; Martinez-Castellanos et al. 2017; Nakahira et al. 2017; Savchenko et al. 2017; Svinkin et al. 2017; Verrecchia et al. 2017; Li et al. 2018). The High Energy Stereoscopic System (H.E.S.S.) array of imaging atmospheric Cherenkov telescopes (IACTs) conducted deep observations in the very-high-energy (VHE; $E > 50$ GeV) gamma-ray regime, achieving upper limits (U.L.s) in the range of 0.13–23.7 TeV (Abdalla et al. 2017). Observations were performed with two different cadences: rapid observations from 0.22 to 5.2 days post-merger, and late-time observations 200 days post-merger (Abdalla et al. 2020). The Major Atmospheric Gamma Imaging Cherenkov (MAGIC) telescopes observed the event between 150 and 300 days after the trigger, achieving a flux U. L. of $3.6 \times 10^{-12}\,\mathrm{erg\,cm^{-2}\,s^{-1}}$ at energies > 0.4 TeV (Stamerra et al. 2022). Notably, the properties of the event, with low interstellar medium density and relatively large viewing angle, were not favourable for VHE detection. However, the detectability of a TeV component from a GW counterpart was hinted by the observation of the short GRB 160821B by MAGIC, although only a 3σ excess was found (Acciari et al. 2021).

Owing to the extraordinary event of 2017, the existence of an EM counterpart of a GW from a BNS merger is no longer a question. On the other hand, no EM counterpart of BBH events has still been observationally confirmed, despite the high number of GW detected (of the order of 100 times greater than BNS events) and different proposed candidates (e.g., Connaughton et al. 2016, 2018; Graham et al. 2020). A significant EM emission from stellar-origin BBH mergers (i.e., both masses of the order of 10–100 $M_{\odot}$) requires particular physical conditions that are still not fully comprehended regarding binary formation channels and the interaction with their environment, nor observationally constrained. One of the most promising channels to produce EM emission is the interaction of the binary or the merger remnant with the gaseous accretion disk of an active galactic nucleus (AGN; e.g., Bartos et al. 2017b; Stone et al. 2017; McKernan et al. 2019). A large number of stellar-mass black holes (BHs) is expected to populate the environment of an AGN as a consequence of dynamical friction-driven migration (Morris 1993; Bartos

[102] https://gwosc.org/eventapi/html/GWTC/

et al. 2013b, 2017b), with both theoretical arguments and observational evidences indicating a number of 2×10^4 BHs within the central parsec (Bahcall & Wolf 1976; Hailey et al. 2018). In this crowded environment, BBH systems can form via dynamical encounters of individual BHs (O'Leary et al. 2009). If a BBH is embedded in the dense and gaseous accretion disk of an AGN, the gravitational merger is accelerated ($\leqslant$1 Myr) and the amplified accretion within the disk can give rise to EM emission (Bartos et al. 2017b; Xue et al. 2025). In this paper, we focus exclusively on the EM emission of BBH mergers embedded in an AGN disk, which should account for 25%–80% of all BBH mergers (Ford & McKernan 2022). Such emission involves X-rays and soft gamma-rays produced by synchrotron radiation from the relativistic jets that are launched after the merger or during the accretion (Bartos et al. 2013a, 2017b). In addition, Kimura et al. (2021) studied the case of kicked BBH mergers, where they identified that at most 10% would have enough kick velocity and kick direction to re-enter the AGN disk and produce EM emission. On the other hand, the synchrotron emission alone cannot produce photons up to tens of GeV, leading to the necessity of additional radiative processes such as inverse Compton scattering. Notably, previous studies on BBH merger counterparts by H.E.S.S. (Abdalla et al. 2021) and VERITAS (Santander 2019) primarily focused on the GRB-like scenario without discussing potential origins of VHE gamma-ray emission.

We report the observations and analysis of two BBH candidates detected by LVK during the O4b run: GW240615_113620 (hereafter, GW240615) and GW241125_010116 (hereafter, GW241125). We followed the two events with the MAGIC telescopes and the Cherenkov Telescope Array Observatory's (CTAO's) first Large-Sized Telescope (LST-1) in stereo-joint configuration, ~14 hr and ~19 hr after the initial trigger, respectively. In both cases, the very good localization of those sources enabled their treatment as point-like sources for observations by IACTs.

This paper is structured as follows: we present the GW data in Section 2 and the observation and analysis of the two events in Sections 3, 4 and 5. Our results are discussed in Section 6. Theoretical models to contextualise our upper limits are discussed in Section 7.3. We draw the final conclusions in Section 8.

2. The Two BBH Events

2.1. GW240615

GW240615 (S240615dg) was identified by the LVK interferometers on the 15th of June 2024 at 11:36:20.724 UTC. This event was immediately classified as a BBH merger with a probability of 99% and a false alarm rate (FAR) of 3.2×10^{-10} Hz (FAR = 1 per 100.04 yr). The luminosity distance, marginalized over the whole sky, is $D_{\mathrm{L}} = 1560^{+290}_{-450}$ Mpc. GW240615 stands as the best localized event of all LVK observing runs, with a 90% confidence area of only 5 deg^2 (LVK Collaboration 2024a, 2024b, 2026a). This event was associated to the merger of two BHs with a total mass of $M_{\mathrm{tot}} = 60.4^{+3.5}_{-2.5}\,M_{\odot}$ (of which $M_1 = 34.0^{+5.4}_{-3.7}\,M_{\odot}$ and $M_2 = 26.4^{+4.0}_{-4.8}\,M_{\odot}$), with an equivalent chirp mass of $\mathcal{M}_{\mathrm{c}} = 25.9^{+1.7}_{-1.2}\,M_{\odot}$. The reported network signal-to-noise ratio is 26.4 (LVK Collaboration 2026a, 2026b).

Taking advantage of the small confidence area, the event was followed up by optical ground-based telescopes (Akl et al. 2024a; Page et al. 2024a; Reguitti et al. 2024) and the Swift space telescope (Evans et al. 2024; Ronchini et al. 2024), although no significant EM counterpart was found in any band. More details about this event can be found in the official GraceDB page.[103]

2.2. GW241125

GW241125 (S241125n) was identified by the LVK interferometers on the 2024 November 25th at 01:01:16.780 UTC with a 90% confidence area of 76 deg^2 (LVK Collaboration 2024c). This event was immediately classified as a BBH merger with a probability of 99% and FAR of 9.5×10^{-10} Hz (FAR = 1 per 33.347 yr). The best estimate of the luminosity distance of the event is $D_{\mathrm{L}} = 4700^{+3900}_{-2200}$ Mpc (LVK Collaboration 2026a). This event was associated to the merger of two BHs with a total mass of $M_{\mathrm{tot}} = 106^{+23}_{-22}\,M_{\odot}$ (of which $M_1 = 60.0^{+14}_{-13}\,M_{\odot}$ and $M_2 = 47^{+14}_{-17}\,M_{\odot}$), with an equivalent chirp mass of $\mathcal{M}_{\mathrm{c}} = 45^{+10}_{-10}\,M_{\odot}$. The reported network signal-to-noise ratio is 11 (LVK Collaboration 2026a, 2026b). More details about this event can be found in the official GraceDB page.[104]

Despite having a very high uncertainty on the distance and localization, this GW represents a good target for EM searches because it originated from BHs in the pair-instability mass gap (if we consider a lower limit of $M_{\mathrm{BH}} \simeq 45 M_{\odot}$; Gerosa & Fishbach 2021). BHs of this kind challenge the current understanding of stellar evolution, and are predicted to be the remnant of a previous gravitational merger (Abbott et al. 2021a; Gerosa & Fishbach 2021; Woosley & Heger 2021), increasing the probability of this BBH to have happened in an AGN disk (Tagawa et al. 2020; Yang et al. 2019; Gerosa & Fishbach 2021).

At the time of the initial detection, GW241125 gained a lot of interest in the community thanks to the putative identification of a sub-threshold EM counterpart by the Swift Burst Alert Telescope (BAT; DeLaunay et al. 2024a; LVK Collaboration 2024c, 2024d). The burst did not pass the automatic repointing criteria of Swift; however, as described in DeLaunay et al. (2024a), the telescope was triggered by the Gamma-ray Urgent Archiver for Novel Opportunities

[103] https://gracedb.ligo.org/superevents/S240615dg

[104] https://gracedb.ligo.org/superevents/S241125n/

(GUANO). Spectral analysis of the putative counterpart revealed a Comptonized spectrum peaking at $E = 49$ keV with photon index −1.2 and a flux in the range between 15 and 350 keV of $1.1^{+0.2}_{-0.3} \times 10^{-7}$ erg cm^{-2} s^{-1} (DeLaunay et al. 2024a, 2024b). Following the initial trigger from Swift, extensive follow-ups by many facilities were performed, however no significant EM counterpart was identified in any band. The INTEGRAL telescope reported an upper-limit of 1.4×10^{-7} erg cm^{-2} s^{-1} in the 75–2000 keV energy band assuming a short GRB spectrum (Savchenko et al. 2024). The Fermi-GBM obtained an upper-limit of 5.5×10^{-7} erg cm^{-2} s^{-1} in the 75–2000 keV energy band (Scotton & Fermi-GBM Team 2024) assuming a hard spectrum, while Konus-Wind yielded an upper-limit of 2.3×10^{-7} erg cm^{-2} s^{-1} in the 10–1000 keV energy band (Ridnaia et al. 2024). A possible X-ray counterpart was detected by both modules of the Einstein Probe Follow-up X-ray Telescope (EP-FXT) at 94 ks after the initial trigger. The position of the X-rays candidate counterpart falls within the 5′ BAT error circle. The derived average unabsorbed flux is $1.17^{+1.18}_{0.63} \times 10^{-13}$ erg cm^{-2} s^{-1} in the 0.5–10 keV band (Wang et al. 2024). The position of the EP-FXT counterpart is consistent with an uncatalogued X-ray source detected by Swift X-ray telescope (XRT) between 55 and 74 ks after trigger, for which a peak flux of $(9 \pm 4) \times 10^{-14}$ erg cm^{-2} s^{-1} was derived in the 0.2–10 keV band (Page et al. 2024b). The afterglow was extensively followed by optical telescopes around the world, although no detection was achieved (Akl et al. 2024b; Becerra et al. 2024; Chen et al. 2024; Jiang et al. 2024; Klingler et al. 2024; Mohan et al. 2024; Rastinejad et al. 2024; Swain et al. 2024; Watson et al. 2024).

3. The Joint VHE Observation Campaigns

The LST-1 is the first telescope of the 23 m diameter telescopes array, designed to be part of the forthcoming CTAO in the Northern Hemisphere (CTAO-N; Cherenkov Telescope Array Consortium et al. 2019). Located at the Observatorio del Roque de los Muchachos in La Palma (Canary Islands, Spain). LST-1 features a reflective surface of approximately 400 m^2 and a camera equipped with high quantum efficiency photomultiplier tubes. The telescope has a field of view (FoV) of 4.3 deg. These characteristics make it particularly well-suited for detecting VHE gamma-rays at the lower end of the spectrum, starting from a few tens of GeV (Abe et al. 2023a).

The MAGIC telescopes are two 17 m diameter IACTs located at the same observatory as the LST-1, sensitive to VHE gamma-rays from around ∼50 GeV up to tens of TeV (Aleksić et al. 2016), with a FoV of 3.5 deg. Despite having a higher energy threshold than the LST-1, the MAGIC telescopes can achieve a better shower reconstruction (energy, direction and background suppression) thanks to the stereo trigger, which allows them to record only events that trigger both telescopes.

The inter-telescope distances, of around 100 m, is comparable to the expected size of the Cherenkov light pool resulting from the extensive shower initiated by a VHE gamma-ray. Therefore, it is possible to combine LST-1 and MAGIC telescopes into a single stereoscopic system, improving the performance and the accuracy of event reconstruction (Kohnle et al. 1996; Abe et al. 2023b).

Observation campaigns searching for counterparts of GW events have been conducted following notably different procedures and selection criteria in the MAGIC Collaboration (Miceli et al. 2019) and LST Collaboration (Carosi et al. 2021). Usually, the GW uncertainty region is much larger than the telescopes' FoV, and therefore a standard observation scheme is not feasible. In the case of LST-1, the observation scheduling is obtained using the so-called *tiling* strategy, relying on the `tilepy` code, described in Seglar-Arroyo et al. (2024). `tilepy` enables the automatic scheduling of follow-up observations by determining the optimal sequence of coordinates to observe, in order to maximize the probability of detection and optimize observation conditions. The scheduling is flexible and can be tailored to either cover the entire uncertainty region or focus only on the most probable areas, depending on the available observation time and configuration. Instead of spending a fixed amount of time on a single set of coordinates, `tilepy` allows distributing that time fractionally across multiple potential positions. This tiling algorithm is being used by other IACTs (e.g., Abdalla et al. 2017) since the beginning of the LIGO–Virgo observing run O2. Similarly, tiling strategies have been consistently used in other wavelengths to address the poor localization of GW events (e.g., see Evans et al. 2016; Ghosh et al. 2016). Recently, the MAGIC and LST Collaborations have set up a joint GW program that enables automatic coordination of observation campaign scheduling, orchestrated by the Transient Handler of LST-1 (Seglar-Arroyo et al. 2025) using `tilepy`.

GW240615 and GW241125 were extraordinary events because, due to the small uncertainty area and the GRB-like candidate identification respectively, the entire region of interest was contained within the telescopes' FoV. Since these events occurred during daytime in La Palma, it allowed for offline coordination of the joint MAGIC+LST-1 observation campaign, marking the first time that observations were scheduled in a coordinated manner between IACTs for a GW event. Given the low localization uncertainty, standard joint wobble observations were identified as the best strategy for both events. In this configuration, the telescopes point alternatively at different directions at a fixed offset from the target (Fomin et al. 1994). Typically, each pointing, or observing run, lasts for ∼20 minutes. This mode allows to define *off-source* regions within the FoV which have the same acceptance as the region around the source, hence facilitating background estimation and minimizing systematic effects related to reconstruction or camera response.

Standalone datasets are reduced with different analysis chains. The standard pipeline for LST-1 data employs the software package `cta-lstchain v0.10.7` (López-Coto et al. 2021; Abe et al. 2023b; Lopez-Coto et al. 2024), while the MAGIC analysis is based on `MARS` (Moralejo et al. 2009; Zanin et al. 2013). To combine the two datasets and perform a stereo analysis, MAGIC data are converted into ctapipe-like data format using the `ctapipe_io_magic` package.[105] The joint analysis is then performed using the `magic-cta-pipe` package.[106] In both cases, the package comes with additional modules for high-level analysis such as `pyirf` (Noethe et al. 2022) for calculation of the instrument response functions (IRFs) and `gammapy` (Donath et al. 2023; Acero et al. 2025) for flux modelling. More details on the joint analysis pipeline can be found in Abe et al. (2023b).

4. Observing Conditions and Data Taking

4.1. Observations of the BBH System GW240615

We observed GW240615 as Target of Opportunity (ToO), with the MAGIC and LST-1 telescopes in stereo configuration. Observations started 14.88 hr after the initial trigger from LVK. LST-1 started observing the event at 2024 June 16 02:29:17 UTC and was followed by MAGIC with 8 minutes delay. The three telescopes observed consistent wobble positions (i.e., with a difference of pointings of less than 0.1 deg) for 111.76 minutes, distributed in 6 observational runs. The observations were simultaneously performed pointing to the first available set of coordinates (*Bayestar* LVK reconstruction, 7.53, +45.81; LVK Collaboration 2024a), although a better localization at 13$'$.49 from the initial one was published a few days later (*Bilby* LVK reconstruction, 7.69, +45.67; LVK Collaboration 2024b).

Observations were performed at a high zenith angle from 65 to 42 deg. Additionally, data-taking was affected by variable night-sky-background (NSB) conditions, although weather conditions during the observations were optimal. Both the level of NSB and the zenith angle have a significant impact on the energy threshold of the telescopes, thus a non-standard approach was necessary to characterize the observations of GW240615. See Appendix A for more information about the energy threshold and the NSB conditions of GW240615 and how we addressed them in our analysis.

4.2. Observations of the Swift-BAT Counterpart Candidate of BBH System GW241125

LST-1 observations of GW241125 started 19.01 hr after the initial trigger from LVK, at 2024 November 25 20:01:49 UTC, and continued for a total of 4 hr. MAGIC observations started with a delay of 29 minutes. Observations were performed in wobble mode around the Swift-BAT candidate coordinates (58.079, +69.689 deg; DeLaunay et al. 2024a). In total, the three telescopes collected data in joint configuration for 201.56 minutes. The zenith angle of the observations went from 55 to 40 deg.

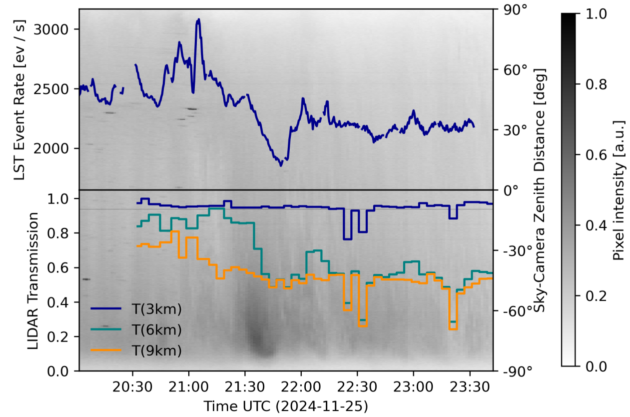

Figure 1. The top plot shows the LST-1 event rates over the night. The bottom plot shows the atmospheric transmission from different altitudes at ground level as determined by the MAGIC LIDAR for the observation of GW241125. The keogram taken at the same time at GTC (∼500 m away from MAGIC) is displayed in the background, with the zenith distance angle of the SkyCamera position. Clouds were present throughout the night, with particularly thick layers appearing after 21:30 UTC. These led to a sharp drop in atmospheric transmission, degrading the data quality to the point where meaningful analysis was no longer possible.

The observation conditions were suboptimal. A Light Detection and Ranging (LIDAR) system has been deployed by the MAGIC collaboration for the monitoring of atmospheric conditions during regular observations (Schmuckermaier et al. 2023). During the observations of GW241125, LIDAR measured vertical atmospheric transmission from 9 km above ground level decreasing from 0.8 to 0.4 due to a persistent layer of clouds. The clouds left only very narrow and sporadic windows of clear sky throughout the night. Due to these poor atmospheric conditions, the data could not be analysed using standard methods and most of them were excluded from the final analysis. To better assess atmospheric quality, we examined the LIDAR and the *keogram* data from that night. The keogram is a plot showing the temporal evolution of brightness along a fixed image slice (usually north–south) from All-Sky camera images (Figure 1). In this case, the keogram was provided by the GTC All-Sky camera.[107] Both monitoring tools show consistent behaviour: the atmospheric transmission at 6 km measured by LIDAR drops simultaneously with the appearance of a thick cloud in

[105] https://github.com/cta-observatory/ctapipe_io_magic
[106] https://github.com/cta-observatory/magic-cta-pipe
[107] https://atmosportal.gtc.iac.es/

the keogram, indicating a sudden deterioration of atmospheric conditions. We select the windows with higher transmission resulting in a total of 19.72 minutes of joint data and 37.68 minutes of LST-1 data, and we set a conservative energy cut of 0.5 TeV. A detailed description of the cut selection procedure can be found in Appendix A.

5. Methodology

5.1. Low-level Analysis

We analysed the data taken with LST-1 in standalone mode using `lstchain` (Abe et al. 2023a) as the main reconstruction framework, and `magic-cta-pipe` (Abe et al. 2023b) for the stereo reconstruction. The procedure starts from the measured charge values, which are corrected, integrated, and cleaned to produce calibrated images. These images are then parametrized, producing Hillas parameters (Hillas 1985). A random forest algorithm is applied to estimate the event energy, arrival direction, and a classification parameter (*gammaness*) that separates gamma-like events from background-like events.

5.2. Sources with Uncertain Localization

We describe here the methodology used to analyse sources with uncertain localization, specifically in cases where the positional uncertainty exceeds the point-spread function (PSF) of the telescope. This approach is applied to the BBH event GW240615, which has not been associated with any known galaxy.

The estimation of the background is critical for IACTs: even after the selection of gamma-like events, the rate of residual background from showers initiated by charged cosmic rays is typically comparable or larger than the rate of gamma-rays from the majority of sources. We used the background modelling tool `pybkgmodel`[108] (Strzys et al. 2023). A cross-check of the results was performed using a different tool, `BAccMod`.[109] Background is estimated using a "3D" model (not assuming radial symmetry), and computed run-wise. In addition, we used the *ring background method* (Berge et al. 2007) to normalize the model over the dataset.

After background modelling, we defined the respective ON and OFF regions to compute Li&Ma significance (Li & Ma 1983) and the flux estimators (Hearn 1969). In the flux calculations, we set a minimum flux of 0 allowed to likelihood estimation. We did not consider negative statistical fluctuations for the flux computation (see details in Appendix B).

Finally, we used the `ExcessMapEstimator` tool provided by the `gammapy` framework to generate the final results (significance and U.L.s) in the form of a sky-map. Since the output represents the integrated flux within a specific correlation radius, we applied a correction factor to account for the fraction of the signal of a point-like source contained within that region (see Appendix B). For GW240615, we chose correlation radii consistent with the PSF of the instrument: specifically, we used 0°.25 for the low-energy analysis and 0°.1 for the higher-energy analysis, both described in Section 6.

5.2.1. Global Statistical Measures using GW Localization

We can combine the information from the LVK observation (the 2D sky-map of the GW event localization) with the gamma-ray data to obtain a single "global" value for the significance, and another one for the flux upper limit (instead of the sky-maps of such quantities). Several approaches have been proposed to address this problem: some rely on a Bayesian framework (I. Bartos et al. 2019; Veske et al. 2020; Abbasi et al. 2023), others adopt a frequentist perspective (Baret et al. 2012; Hussain et al. 2020), while a third class of methods takes a hybrid approach combining elements of both (Vianello et al. 2017).

For this project, we adopted a frequentist approach following Hussain et al. 2020 (see the full scheme in Figure 2). We modify the standard test statistics (TS) used for significance computation (Li & Ma 1983), which for each pixel i is defined as the Likelihood Ratio Test between the two Poisson likelihood hypothesis:

$$\mathrm{TS}_i = 2\log\left(\frac{\mathcal{L}_i^{\mathrm{source+BKG}}}{\mathcal{L}_i^{\mathrm{BKG}}}\right). \tag{1}$$

Following Hussain et al. (2020), we define the modified test statistic TS′ by weighting the likelihood with the GW prior spatial information in each pixel (i.e., the 2D probability map of GW localization). In this way, we are also incorporating the information from the LVK likelihood by integrating it over each pixel. Since the GW and gamma-ray data are independent, and the standard likelihood is already integrated in the first part, the combined likelihood can be expressed directly as the product of the individual likelihoods. We use WCS geometry (Donath et al. 2023; Greisen et al. 2003), with square (in R.A.-decl.) bins with slightly different solid angle between them. The LVK sky-map of probabilities is provided in HEALPix coordinates (Górski et al. 2005). The integrated probability per WCS pixel, P_i^{GW}, is obtained by summing the HEALPix pixels contained within each WCS pixel and normalizing by their areas. With a resolution of about 12 HEALPix pixels per WCS pixel, the transformation maintains fidelity to the original map

$$\mathrm{TS}_i' = 2\log\left(\frac{\mathcal{L}_i^{\mathrm{source+BKG}}\cdot P_i^{\mathrm{GW}}}{\mathcal{L}_i^{\mathrm{BKG}}}\right) = \mathrm{TS}_i + 2\log\left(P_i^{\mathrm{GW}}\right). \tag{2}$$

[108] https://github.com/cta-observatory/pybkgmodel
[109] https://github.com/mdebony/BAccMod

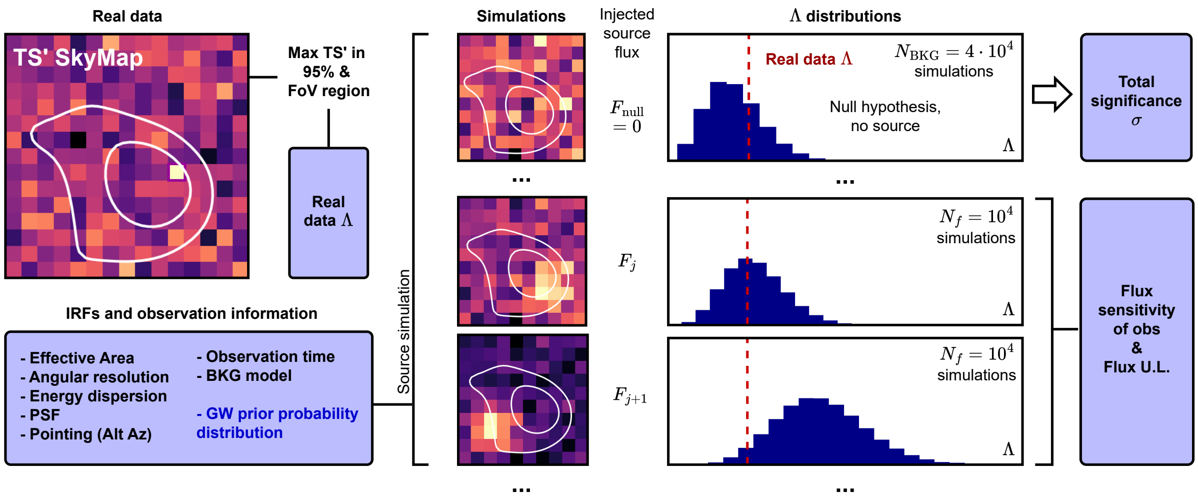

Figure 2. Schematic representation of the frequentist parameter estimation workflow. From left to right: (1) Real Data: Gamma-ray data (skymap) is combined with the GW spatial prior (white contours) to generate a modified test statistic map, TS′. The maximum value within the overlap of the 95% GW localization and the instrument FoV is defined as the observed statistic, $\Lambda_{\rm data}$. (2) Simulations: Toy MC realizations are generated using the relevant IRFs and observation metadata. These include a null-hypothesis set ($F_{\rm null} = 0$) and multiple sets with injected source fluxes ($F_{\rm j}$) sampled from the GW prior. (3) Λ distributions: The resulting probability density functions of Λ for each simulation set are compared against $\Lambda_{\rm data}$ (red dashed line). (4) Results: These comparisons yield the total significance (σ), global flux U.L., and the flux sensitivity of the specific observation. See text for more details.

The search of the largest TS′ is then restricted to the overlap between:

1. The 95% containment region of the GW localization, based on the LVK prior. Although some works (e.g., Vianello et al. 2017) use 90%, we adopt 95% to maximize the observed data used in the analysis.
2. The region covered by the observations. Different criteria may be adopted, such as a constant search radius or an exposure threshold. In the present case, since the entire 95% region is above the 30th percentile of the nonzero exposure distribution, we consider that is well covered (see more details in Appendix A).

Within this overlap region, we identify the maximum value of TS′, which we denote as the derived test statistic, Λ. To understand the distribution of Λ under the null hypothesis, we use toy MC simulations produced with `gammapy` (Donath et al. 2023; Acero et al. 2025). These simulations use the same IRFs and background (BKG) models as the analysis, along with the pointing information and time and date of observations. Comparing the observed Λ to the null distribution for $N_{\rm BKG}$ simulations (in our case, we used $N_{\rm BKG} = 40{,}000$), the p-value is computed as the fraction of events with larger Λ than the observed $\Lambda_{\rm data}$. The significance (in units of σ) is, instead, estimated using the inverse cumulative distribution function of the standard normal distribution: $\Phi^{-1}(1 - p\text{-value})$.

In addition, multiple simulations are produced for a range of flux values, with $N_f = 10{,}000$ realizations for each. Each realization consists of a toy MC injecting a source at a random sky position drawn from the GW probability distribution. In our analysis, the source was modelled by a power-law with spectral index −2. For each value of amplitude, we computed N_f realizations. We choose amplitude values equally spaced in logarithmic scale, with 40 bins per decade, from $\times 10^{-14}$ to $\times 10^{-9}$ erg cm^{-2} s^{-1}. We ignore the cases where the simulated source falls outside the 95% containment region. Consequently, if only a fraction F of the GW localization region is observed, our results carry an inherent uncertainty of $1 - F$. The reported upper limits are therefore conditional on the assumption that the GW source lies within the observed region.

We aim to determine the sensitivity of the observations, i.e., the minimum flux that would have been detected by the method for a given set of observations. Following a similar approach to other works (Vianello et al. 2017; Hussain et al. 2020), we define the U.L. as the flux for which 95% of trials yield a Λ value larger than the one of the real data, i.e., $\Lambda_f > \Lambda_{\rm data}$. If the observed $\Lambda_{\rm data}$ is smaller than $\Lambda_{\text{bkg-median}}$, the median of the null hypothesis distribution, or equivalently, if the total significance is negative, this indicates a downward fluctuation of the background: in such cases, we take a conservative approach. We define the sensitivity of our observations as the flux for which 95% of trials yield a Λ value larger than $\Lambda_{\text{bkg-median}}$, i.e., $\Lambda_f > \Lambda_{\text{bkg-median}}$. We use the sensitivity of the observations as a U.L. in those cases. The global U.L.s presented have therefore a 95% confidence level (CL), in addition to the implicit assumption of the source being located in the 95% GW probability region, resulting on a global CL of 90%.

5.3. Analysis of Localized Sources in Suboptimal Weather Conditions (GW241125)

As discussed in Section 5 the observations of GW241125 were affected by suboptimal weather conditions, including a thick layer of clouds, as indicated by LIDAR measurements and by telescope rates, that are ∼60% lower than optimal values (Figure 1). Most of the data were discarded for quality reasons, but also the remaining dataset is far from optimal, with event rates ∼40% lower than in normal, clear and dark-sky conditions. To maximize the scientific return from these observations, we performed a tailored analysis specifically optimized for the atmospheric conditions during the observations.

The atmosphere, while essential to the detection process, is also an important source of systematic uncertainties. The extinction of Cherenkov radiation due to scattering and absorption by aerosols and cloud layers can significantly reduce the number of photons reaching the telescopes, thereby decreasing the Cherenkov light yield and the effective collection area (Bernlöhr 2000; Sobczynska & Bednarek 2014; Pecimotika et al. 2023). Consequently, if these effects are not taken into account, a systematic underestimation of both the reconstructed primary gamma-ray energy and flux may occur (Schmuckermaier et al. 2023; Żywucka et al. 2024).

We generated adapted MC simulations following the approach presented in Pecimotika et al. (2023). The central idea of this approach is to calibrate the telescope response according to the prevailing atmospheric conditions. To this end, MC simulations are produced using dedicated atmospheric transmission profiles, specifically incorporating cloud properties derived from measurements with atmospheric monitoring instruments such as the LIDAR system. This allows to model the impact of clouds on the Cherenkov signal detected in the telescope camera. As shown by Pecimotika et al. (2023) and Żywucka et al. (2024), using adapted MC simulations to generate random forest models reduces the energy bias to the levels seen in clean atmosphere observations, without impairing energy resolution.

MC simulations of extensive air showers induced by primary gamma-rays and protons were generated using CORSIKA (Heck et al. 1998), while the subsequent propagation and extinction of Cherenkov photons through the atmosphere, along with the detector response, were simulated using the `sim_telarray` code (Bernlöhr 2008). The table of optical depths needed for calculations with `sim_telarray` was generated using the MODerate spectral resolution atmospheric TRANsmittance (MODTRAN) band model algorithm (Berk et al. 1987). The baseline (clear-sky) atmospheric transmission profile was adapted from the default atmospheric configuration used in the LSTProd2[110] settings for `sim_telarray`, namely using the tropical atmosphere with navy maritime extinction. The cloud layer was integrated into the baseline profile by specifying cloud parameters in the MODTRAN simulations, based on measurements from MAGIC's elastic micro-Joule LIDAR (Fruck et al. 2022). The cloud layer for GW241125 observations was characterized by a vertical transmittance of 0.736, a base height of 6.86 km above sea level, and a total thickness of 3.68 km, assuming wavelength-independent and uniform extinction throughout the cloud (Fu 1996; Serrano et al. 2015). General settings for simulations with CORSIKA and `sim_telarray` for both joint and mono observations are described in Abe et al. (2023a, 2023b), respectively.

[110] https://github.com/cta-observatory/lst-sim-config

6. Results

6.1. GW240615

We divided the data analysis of GW240615 in two energy ranges to account for the varying energy threshold and fully exploit the capabilities of the LST-only and MAGIC+LST-1 configurations (see Appendix A). In particular, LST-only data are analysed in the low-energy range $0.15\,\mathrm{TeV} < E_\gamma < 0.6\,\mathrm{TeV}$, while MAGIC+LST-1 in the high-energy range, $E_\gamma > 0.6\,\mathrm{TeV}$.

For the gamma–hadron separation efficiency—that is, the energy-dependent cuts applied to data and MC simulations to retain a given fraction of gamma-ray events after reconstruction—we adopted values of 50% for the low-energy analysis and 70% for the high-energy analysis. The higher efficiency needed in the high-energy range reflects the improved background suppression provided by stereo observations.

We computed statistical significance sky-maps (see Figure 3 and Appendix C); no significant regions are found above 5σ. Using the method described in Section 5.2.1, we obtained global significance estimates of 1.01σ for low-energy analysis and 1.43σ for high-energy analysis (see also Figure 3).

We also computed the flux sky-maps (Figure 3). All the U.L.s in the sky-map are produced with 95% CL. No significant structures or excesses are visible, and the maps are consistent with statistical fluctuations, in line with the previous significance results. As expected, the upper limits are higher in the regions where the instrument is less sensitive, such as at the edges of the field of view. The corresponding projected distributions for both sky-maps are presented in Figure 4, which also includes the derived flux U.L.s, together with the integrated Crab flux in the energy ranges (from Aleksić et al. 2015). We computed the global flux U.L.s with the method detailed in Section 5.2.1. Results are summarized in Table 1.

6.2. GW241125

For the analysis of GW241125, where a candidate counterpart was identified (DeLaunay et al. 2024a; LVK

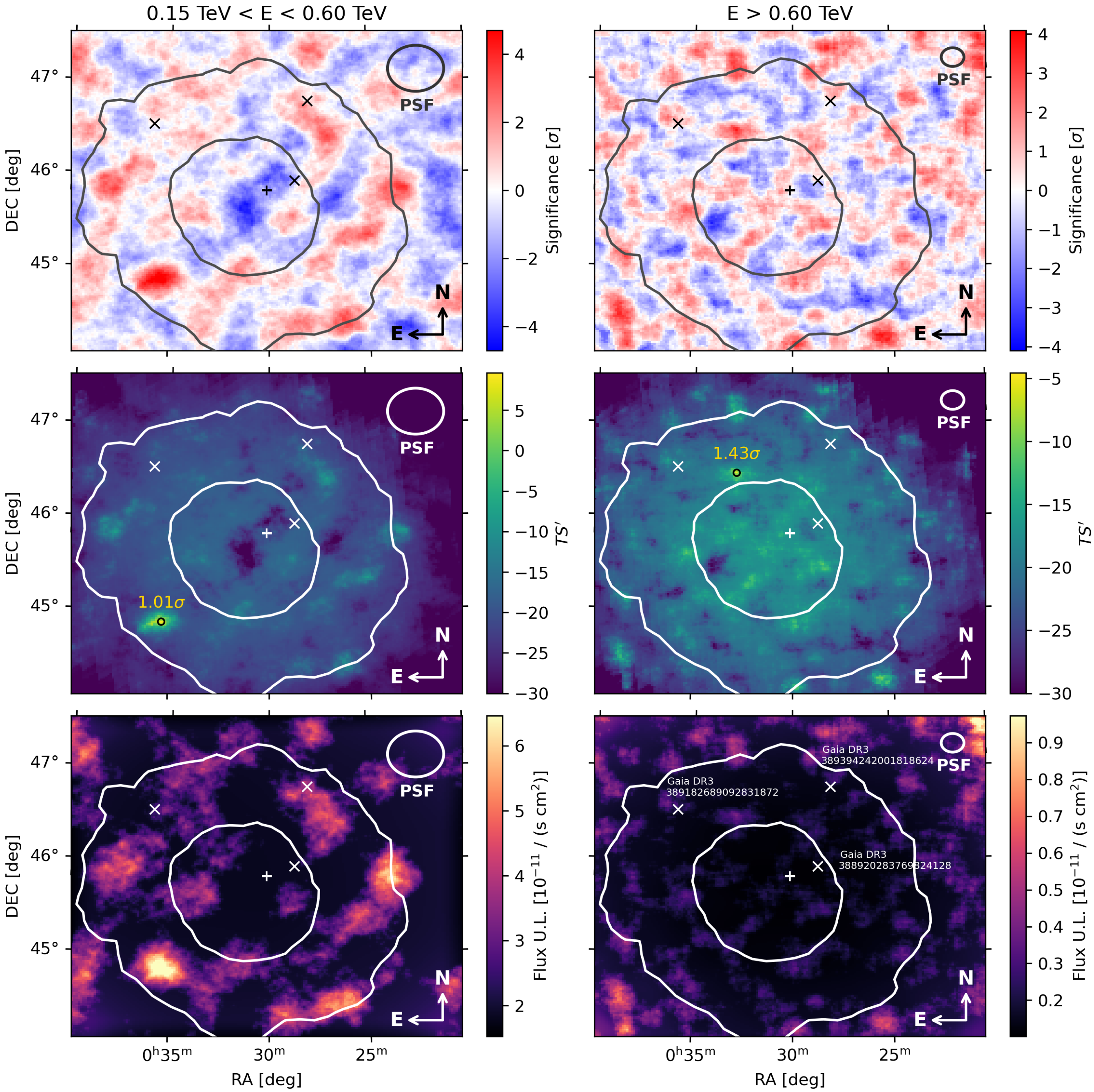

Figure 3. The top row shows the significance sky-maps for GW240615, analysed in both energy ranges. The middle row is showing the TS′ maps (Equation (2)) and the largest significance point of the interest region (with black circles), superposing the resulting global significance on them. The flux U.L. sky-maps for both energy ranges with 95% CL is shown in the bottom row. The contours show 50% and 95% GW containment region, while the cross corresponds to the Bayestar position, i.e., the direction followed by our observations. The PSF (68% containment) averaged over the energy range is indicated in the top-right of each panel. The "x" signs represent the position of the 3D coincident AGNs in the catalogue crossmatch (See Section 7).

Collaboration 2024c, 2024d), no sky-map search was performed. The LVK uncertainty without the candidate counterpart information was too large enough (2196 $\deg^2$) to be observed with IACTs, hence we only observed the small region where the candidate counterpart was located. We computed the significance, the Spectral Energy Distribution (SED) and the Light Curve (LC) treating the GW as a point-like source. The entire analysis was performed using the

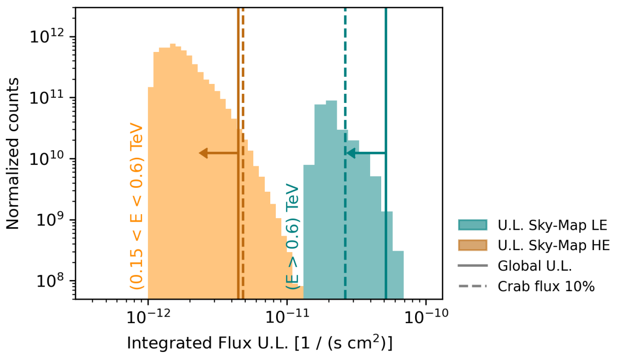

Figure 4. Flux upper limits of GW240615 in the $0.15 < E < 0.6$ TeV (teal) and $E > 0.6$ TeV (orange) energy ranges are shown. The histograms represent the sky-map U.L.s distribution for all the pixels. Vertical solid lines represent the global U.L., derived from the uncertain source localization method described in Section 5.2. Vertical dashed lines represent the 10% of Crab in the corresponding energy range (from Aleksić et al. 2015).

Table 1
Flux Upper Limits of GW240615

Energy Range (TeV)	Significance (σ)	U.L. (cm^{-2} s^{-1})	U.L. (% C.U.)
$0.15 < E < 0.6$	1.01	5.17×10^{-11}	19.7
$E > 0.6$	1.43	4.47×10^{-12}	9.2

Note. Upper limits are computed for the LST-1 ($0.15 < E < 0.6$ TeV) and for the MAGIC+LST-1 ($E > 0.6$ TeV) energy ranges. We used a confidence level of 95%. Values are reported in cm^{-2} s^{-1} and percentages of Crab Units (% C.U.).

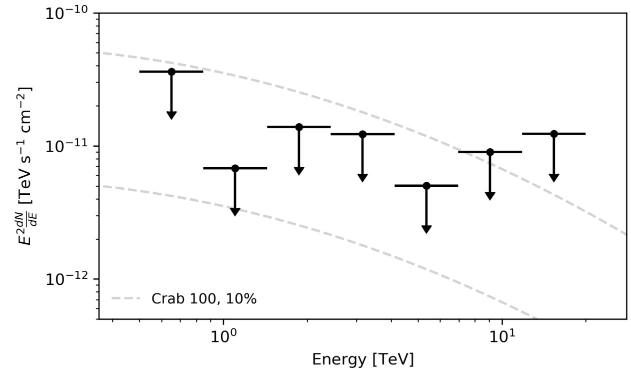

Figure 5. SED calculated for the candidate counterpart position of GW241125. The source was not statistically detected in any of the energy bins. The 100% and 10% MAGIC Crab SED are also plotted for comparison (Aleksić et al. 2015).

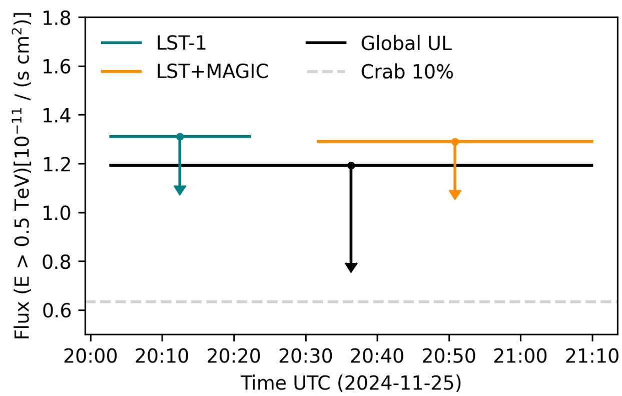

Figure 6. The LC of the observations of GW241125 for energies larger than 0.5 TeV. It has been separated in 3 runs of about 20 minutes, where we distinguish between the run that was taken with LST-1 in mono mode and the ones taken in stereo mode with MAGIC+LST, that are shown as a unique limit in the plot. We also show the global U.L. using stacked data.

standard `gammapy` tools (Donath et al. 2023; Acero et al. 2025). The CL of the U.L.s provided both in the SED and the LC are 95%.

We computed the distribution of separations of reconstructed events to the source position for ON and OFF regions (see Appendix C) obtaining statistical significance of 2.2σ for LST data and 1.47σ for LST+MAGIC data. The SED and the LC are computed for reconstructed energies $E >$ 0.5 TeV and are shown in Figures 5 and 6, respectively. The light curve was computed using a power-law spectral model with a fixed index of $\alpha = -2$. Since the first observation run was performed with LST-1 alone, the resulting limits are expected to be weaker, reflecting the reduced sensitivity of mono reconstruction compared to the stereo reconstruction. The differences seen between LC points, correspond to statistical fluctuations: lower significances yield tighter U.L.s and vice-versa. Overall, the derived limits are consistent with each other. From approximately 1 h of observations, combining the individual likelihoods, we obtain a global flux upper limit of 1.2×10^{-11} s^{-1} cm^{-2}.

7. Discussion

The two sources presented in this paper offered an unprecedented opportunity to observe a compact binary coalescence with gamma-ray ground-based telescopes. Although no gamma-ray signal was detected, the derived upper limits allow discussing current theoretical frameworks that predict a detectable VHE flux. In this regard, we exclusively focus on models of BBH mergers embedded within AGN disks, as these environments offer the necessary conditions for accelerating particles to VHE energies, unlike the case of isolated systems. Specifically, we discuss two models, both of them requiring accretion and subsequent jet launching, and predicting strong EM emission temporally coincident with the GW signal. We also consider the implications for future observational facilities and the observability by current telescopes. Additionally, we explore

AGN association. It is important to note that a detailed theoretical interpretation of these events is beyond the scope of this manuscript. Therefore, our discussion relies on strong assumptions and physical conditions proposed in the existing literature.

7.1. Super-Eddington Accretion

Accretion of gas onto a BH in a binary system is a well established mechanism that allows the production of an EM signature, detectable at high energies (Shakura & Sunyaev 1973; Abramowicz & Fragile 2013; Belloni & Motta 2016; Bambi & Santangelo 2024). If the rate of accretion is larger than a critical value $\dot{M}_{\rm Edd}$, corresponding to a limit luminosity $L_{\rm Edd}$, the radiation force will exceed the gravitational force, driving fast and high energetic outflows (Jiang et al. 2014; McKinney et al. 2014; Murase et al. 2016). One of the most compelling evidence of super-Eddington accretion are the ultra-luminous X-ray binaries, which can exceed by 10–1000 times the Eddington limit depending on the mass of the compact object (e.g., Begelman 2002; Farrell et al. 2009; Pinto & Walton 2023). Given that the accretion mainly depends on the presence and properties of a gaseous disk around the BH, a similar mechanism is proposed for BBH systems embedded in the accretion disk of an AGN (e.g., Bartos et al. 2017b; Stone et al. 2017). In this environment, the merger is accelerated by loss of angular momentum of the binary due to viscous friction with the gaseous disk, resulting in mergers in less than 1 Myr (Bartos et al. 2017b). The binary may accrete significant amount of gas from the AGN disk, which can exceed the Eddington limit producing outbursts. In proximity of the merger, the escaping flux can be enhanced by several orders of magnitude compared to similar mass BHs thanks to shocks produced by the orbital motion of the binary (B. D. Farris et al. 2010). In particular, Bartos et al. (2017b) discussed a geometrically thin, optically thick, radiatively efficient and steady-state accretion disk, as expected in AGNs (Shakura & Sunyaev 1973). If the BBH is buried within the disk, emission can be reprocessed, effectively losing energy to the disk. This would result in an optical/IR signature spread in time. If, instead, during the spiralling phase, the binary has created some open gaps within the AGN disk (e.g., Duffell 2015; Bartos et al. 2017b), the high-energy emission can pass through and be detected on Earth. The timescale of this emission varies from hours to days depending on the mass of the remnant, the accreting mass along the orbit of the BH and the mass accretion rate (e.g., Murase et al. 2016). Bartos et al. (2017b) defined the detectability of high-energy emission from the accreting binary by modelling the observed flux as a function of the super-Eddington efficiency. They define:

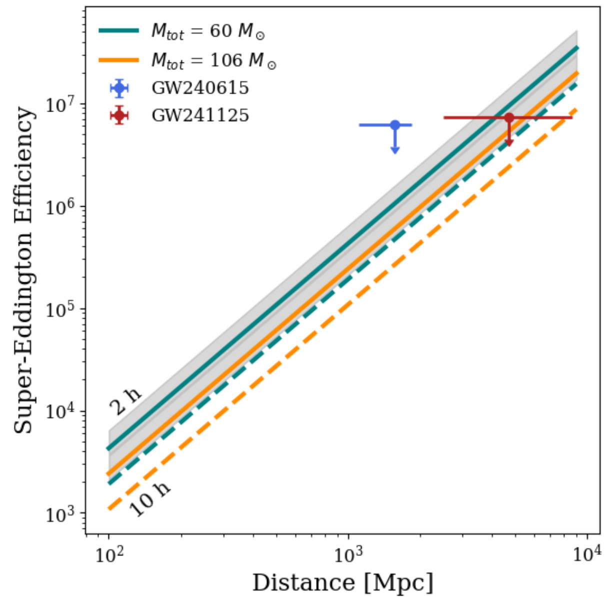

Figure 7. Super-Eddington efficiency $\eta_{\rm bol}$ evolution with distance. Diagonal lines represent the efficiency lower limits considering the sensitivity of MAGIC+LST-1 at 500 GeV with 2 hr (thick solid lines) and 10 hr (dashed lines) of integration at zenith angle < 30 deg (Abe et al. 2023b). The gray bands cover the sensitivity area between 0.3 and 8 TeV. Efficiency is estimated with two possible $M_{\rm tot}$, 60 $M_\odot$ (orange) and 106 $M_\odot$ (green), and assuming a partition factor of $\epsilon_\gamma = 0.1$. For comparison, we plot the GW240615 ($M_{\rm tot} \sim 60.4 M_\odot$ and $D_{\rm L} = 1560^{+290}_{-450}$ Mpc) and GW241125 ($M_{\rm tot} \sim 106 M_\odot$ and $D_{\rm L} = 4700^{+3900}_{-2200}$ Mpc) upper-limits.

$$\Phi_\gamma = 10^{-14}\eta_{\rm bol}\,\epsilon_\gamma\left(\frac{M_{\rm tot}}{100 M_\odot}\right)\left(\frac{D}{100\ {\rm Mpc}}\right)^{-2}\ {\rm erg\ s^{-1}\ cm^{-2}} \quad (3)$$

where Φ_γ is the observed flux in gamma-rays, $\eta_{\rm bol} = L_{\rm bol}/L_{\rm Edd}$ is the super-Eddington efficiency, $\epsilon_\gamma = L_\gamma/L_{\rm bol}$ is the fraction of the bolometric luminosity $L_{\rm bol}$ emitted in gamma-rays. Note that Bartos et al. (2017b) discussed the observability of such emission solely within the energy ranges of the Chandra and Fermi space telescopes.

Using Equation (3) with the masses, the distances and the flux upper-limits of GW240615 and GW241125, and assuming $\epsilon_\gamma = 0.1$, we constrain the super-Eddington efficiency of these sources. We obtained $\eta_{\rm bol} \leqslant 6.3 \times 10^6$ and $\eta_{\rm bol} \leqslant 7.4 \times 10^6$, respectively. Additionally, we use the sensitivity curves of the MAGIC+LST-1 configuration to put a lower-limit on the super-Eddington efficiency necessary to detect a gamma-ray signature with our telescopes. With 2 and 10 hr of exposure at 500 GeV, the MAGIC+LST-1 are able to reach a flux of $\sim 2.6 \times 10^{-12}$ erg cm^{-2} s^{-1} and $\sim 1.2 \times 10^{-12}$ erg cm^{-2} s^{-1}, respectively Abe et al. (2023b). These correspond to a super-Eddington efficiency lower-limit of the order of $\eta_{\rm bol} \geqslant 10^5$ at $d =$ 1000 Mpc, and of $\eta_{\rm bol} \geqslant 10^6$ at $d =$ 4000 Mpc. Note that these estimates are obtained assuming that the emission is distributed isotropically. Results are shown in Figure 7.

These values are at least three orders of magnitude above the super-Eddington luminosity that is expected to be achievable in these systems (Jiang et al. 2014; McKinney et al. 2014; Murase et al. 2016). Therefore, it would have been impossible to detect any of the two sources in absence of strong beaming effects capable of boosting the effective luminosity by some orders of magnitude (Bartos et al. 2017b). However, the prospect of detection improves significantly when reducing the distance of the merger. For instance, at 100 Mpc we could detect a source with $\eta_{\rm bol} \sim 10^3$ with only 2 hr of exposure.

7.2. Post-Merger Jet

While the super-Eddington framework discussed in Section 7.1 provides a direct insight into the energetics of the system based on a simplified parameterization, it does not model the specific physical mechanisms generating the multi-wavelength spectrum. To complement this broad constraint, we now consider a highly detailed model, based on the work by (Tagawa et al. 2023).

When an accreting BH is rapidly spinning in a highly magnetized medium, a jetted emission occurs, labelled Blandford–Znajek (BZ) jet (Blandford & Znajek 1977; Tagawa et al. 2022). As the jet collides with gas it forms strong forward and reverse shocks, where photons are initially trapped due to scattering processes. Eventually, as the shock approaches the disk surface, photons start to escape and electrons are efficiently accelerated producing non-thermal emission via synchrotron and inverse Compton scattering processes, whereas the second- and third-order inverse Compton scatterings are suppressed by the Klein-Nishina effect.

Shock breakout emission from a BBH system is expected to be produced even before the merger, as the jet can be efficiently launched by a single accreting BH. However, catching such emission without any prior information on the localization of the BBH and the nature of it is challenging—if not impossible. Hence, observations must be triggered by a GW signal. In this regard, Tagawa et al. (2023) tailored a theoretical framework that accounts for both thermal and non-thermal emission from the collision of a BZ jet emitted after merger with the un-shocked gas of an AGN disk. The key element is that the post-merger jet produced by the remnant BH has to be launched with a different orientation with respect to pre-merger jets in order to interact with un-shocked gas and trigger shocks. This is possible because before the merger each BH's spin tends to be aligned perpendicularly to the AGN disk, while, during the merger, the binary's orbital angular momentum is generally randomized due to frequent binary–single interactions and inhomogeneities in the disk. As a result, the remnant BH will acquire a new spin orientation, different from the pre-merger alignment, and the shock breakout emission will follow the GW signal.

This process is regulated by two timescales: the delay time between the emission of a jet and the consequent breakout emission ($t_{\rm delay}$) and the duration of emission from a breakout shell ($t_{\rm duration}$). In non-relativistic regimes, the former coincides, with the time delay between the GW and the breakout, and the latter with the duration of the bright emission itself. In relativistic regimes, and when shocks are propagating toward the observer, the breakout timescale is reduced due to the beaming effect, to pair-production, and to the Klein-Nishina effect. These timescales are particularly sensible to the properties of the AGN disk, its density profile and the radial distance R of the BBH from the central super-massive black hole (SMBH). In particular, the duration of the emission scales as $t_{\rm duration} \sim R^3$, with the consequence that BBHs located further from the SMBH have a higher probability to be detected following a GW alert. This is because the usual time of pointing a ground-based telescope ($\sim$ 1 day) is shorter than the expected duration of mergers at $R \geqslant 1$ pc of $\sim$ weeks. The authors refer the readers to Tagawa et al. (2023) for further details on the assumptions and physical parameters for this model.

Figure 8 shows an example of the predicted SED from a BBH merger with $M_{\rm tot} = 120 M_\odot$ evaluated at the distance of GW241125 for two values of radial distance from the central SMBH (1 and 0.01 pc), corresponding to two values of duration of the emission (10^5 and 30 s). For comparison, we plot the observed flux and flux upper-limits obtained with the Swift-BAT, INTEGRAL, Fermi-GBM and Konus-Wind telescopes in the (rest-frame) timescale between $T_0 + 6.8$ s and $T_0 + 8$ s, with the Swift-XRT and EP-FXT telescopes between $T_0 +$ 55 ks and $T_0 +$ 94 ks, and the upper-limits obtained with MAGIC+LST-1 at $T_0 +$ 32 ks. Following the same nomenclature used for gamma-ray bursts, we define as "prompt" the observations performed a few seconds after the GW signal and "afterglow" the observations performed hours to days after the GW signal. This distinction, however, is just conventional: the signal should not have changed drastically over the entire duration of observations if $t_{\rm duration} \sim 10^5$ s.

The observed $t_{\rm delay}$ of the Swift-BAT detection is (in the rest-frame) $11.264/(1 + z) \approx$ 6.47 s (DeLaunay et al. 2024a; Zhang et al. 2026), while the $t_{\rm duration}$ of the emission can be assumed to be equal to the time-bin in which the burst was identified, i.e., 0.512 s. These information, combined with the AGN properties constrained by Zhang et al. (2026), indicate that the BBH merger was likely located deep into the AGN disk, at $R \leqslant 10^2$ pc. Moreover, the Swift-BAT flux lies significantly above the expectations from the thermal emission model in the $R = 10^2$ pc scenario, suggesting that the BBH merging location was even deeper inside the disk. These findings drastically reduce the possibility of a detection of

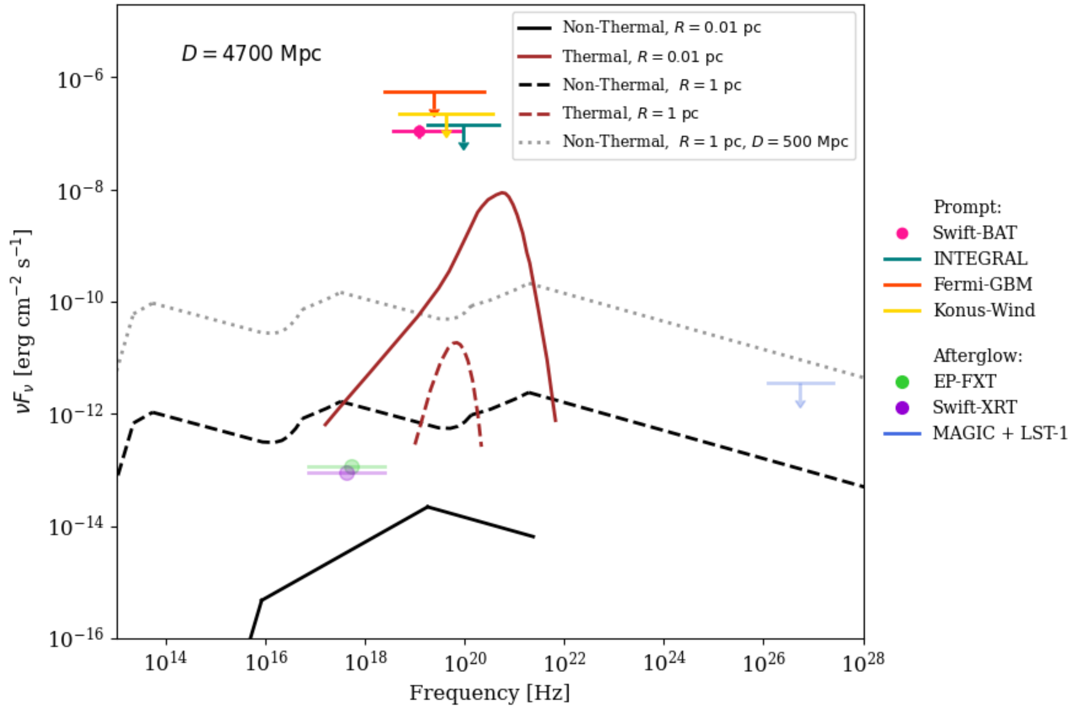

Figure 8. SED of thermal (brown) and non-thermal (black) emission from the post-merger shock in the case of a BBH system with a total mass of $M_{\rm tot} = 120\, M_\odot$ at 4700 Mpc from the observer. The solid lines represent the case with $R = 10^{-2}$ pc and $t_{\rm duration} = 30$ s, and the dashed lines the case with $R = 1$ pc and $t_{\rm duration} = 10^5$ s. Additionally, we plot the non-thermal emission at 500 Mpc and $R = 1$ pc in light dotted black. We show flux points and upper-limits obtained during the prompt-phase (i.e., a few seconds after the GW signal) with Swift-BAT (DeLaunay et al. 2024b), INTEGRAL (Savchenko et al. 2024), Fermi-GBM (Scotton & Fermi-GBM Team 2024), and Konus-Wind (Ridnaia et al. 2024). For completeness, we also show the X-ray candidate counterpart fluxes reported by EP-FXT (Page et al. 2024b) and Swift-XRT (Wang et al. 2024) during the afterglow (i.e., hours or days after the GW signal), together with our MAGIC+LST-1 deepest upper-limit. Afterglow measurements are displayed with a lighter tone to distinguish them from the prompt observations. This figure was adapted with courtesy from Tagawa et al. (2023).

VHE gamma-rays with the MAGIC+LST-1 telescopes. In fact, even if the observations were conducted during the prompt emission, the flux would have been orders of magnitude dimmer than the telescopes' sensitivity. Moreover, we note that this model is somehow optimistic: gamma-ray flux at GeV–TeV energies can be severely obscured by $\gamma{-}\gamma$ annihilation if the Lorentz factor of the jet is not sufficiently high (i.e., $\Gamma \sim 30$; Tagawa et al. 2023; also, since the peak of the observed emission lies in the X-ray regime, the VHE flux is expected to be highly suppressed by the Klein-Nishina effect, further diminishing the expected flux (see for example Figure 2 of Tagawa et al. 2023). Additionally, even if the flux was strong enough to exceed the detection threshold, several observational challenges would remain. These include complicating environmental effects such as torus obscuration, gas properties, and beaming (Tagawa et al. 2023, 2024). Nevertheless, according to this model, emission from a merger occurring at ∼500 Mpc and within $R \geqslant 1$ pc could, under favourable conditions, be detectable from Earth.

7.3. AGN Association

The identification of a host galaxy or AGN counterpart to a GW event relies on the completeness of the candidate catalogues available. For both events several catalogues were investigated: GLADE+ (optical/near-IR; Dálya et al. 2022), Quaia (optical/near-IR; Storey-Fisher et al. 2024), MILLIQUAS v8 (optical; Flesch 2023), and MORX v2 (radio/X-ray association catalog; Flesch 2016). Note that the redshift present in most of those big catalogues is photometric, which implies a factor 100 larger than spectrometric redshifts, affecting the association reliability. We also searched the Fermi-LAT 4th source catalogue (Abdollahi et al. 2020), finding no high-energy sources for any of the regions.

Considering a fiducial AGN number density $\rho_{\rm agn} = 10^{-4.75}\,{\rm Mpc}^{-3}$ (Greene & Ho 2009; Bartos et al. 2017a), a total of ∼30 AGN are expected in the GW240615 95% volume. Despite the precise 2D localization of GW241125, its distance uncertainty leads to a comparable expectation of ∼10 AGNs within the search volume.

Table 2
The Three AGN Candidates Identified within the 95% Localization Volume of GW240615

Gaia DR3 Source ID	R.A. (deg)	Decl. (deg)	$z_{\rm phot}$	$D_{\rm L}$ (Mpc)	Int. prob.	Flux UL $0.15 < E < 0.6$ TeV	Flux UL $E > 0.6$ TeV
388920283769824128	7.18	45.91	0.27(7)	1434(413)	0.37	1.8×10^{-11}	1.1×10^{-12}
389394242001818624	7.01	46.77	0.34(10)	1840(623)	0.89	2.4×10^{-11}	2.3×10^{-12}
389182689092831872	8.96	46.52	0.33(13)	1818(791)	0.83	3.7×10^{-11}	1.5×10^{-12}

Note. IDs and coordinates are from Gaia DR3 (Gaia Collaboration et al. 2023) and unWISE (Schlafly et al. 2019). Photometric redshifts ($z_{\rm phot}$) are from the Quaia catalog. Luminosity distances ($D_{\rm L}$) were computed assuming a flat ΛCDM cosmology with $H_0 = 67.4$ km s^{-1} Mpc^{-1} and $\Omega_{\rm m} = 0.315$ (Planck Collaboration et al. 2020). We also report the integrated 2D probability of association with the GW event and the flux upper limits for each source.

Galactic extinction and stellar crowding at low galactic latitudes ($-16\overset{\circ}{.}9$ and $12\overset{\circ}{.}1$ respectively) limit the completeness of extragalactic catalogues for GW240615 and GW241125. In the case of the first one, the 95% localization volume yielded 3 AGNs and ∼2000 field galaxies. This is ∼10% of the expected density of both, confirming a deficit in catalogue completeness. In the case of GW241125, given the proximity to galactic plane and larger distance, no AGNs or galaxies are found in the 95% volume.

Despite the catalogue incompleteness, the crossmatch for GW240615 identified 3 AGNs, all from Quaia catalogue. Details of these 3 sources in Table 2 (also show in Figure 3). None of the identified candidates spatially coincide with any localized region of elevated significance. Recent estimates based on comparisons to the observed BH masses, spins, and merger rate, suggest that BBH mergers happening inside of AGN disk can contribute to 25%−80% of all GWs detected by LVK (Ford & McKernan 2022). Given the observed deficit in catalog completeness near the galactic plane and the lack of candidates for GW241125, and the uncertainty in the redshift, we cannot definitively claim nor exclude that either event originated within an AGN disk.

8. Conclusions

We presented VHE follow-up of two GW candidates, GW240615 and GW241125. The sources were observed with the MAGIC and CTAO LST-1 telescopes both in standalone and stereo joint configurations, operating in a standard wobble mode, which allowed the longest on-source search of EM counterpart candidates in the VHE band ever obtained with IACT systems. GW240615 was the best localized event of all LVK runs, with a region of uncertainty of only 5 deg^2, smaller than the FoV of the MAGIC and LST-1 telescopes. GW241125 was the only event during O4 with a putative EM candidate detected with the Swift-BAT telescope during the prompt emission and with the Swift-XRT and EP-FXT during the afterglow. No detection was achieved in the GeV–TeV band for any of the two sources. In the case of GW240615, we used an existing method to combine the observation significance sky-map and the GW probability area to achieve a single limit. We obtained 5.17×10^{-11} cm^{-2} s^{-1} in the 0.15–0.6 TeV energy range and 4.47×10^{-12} cm^{-2} s^{-1} above 0.6 TeV. In the case of GW241125, we performed a tailored analysis for sources with suboptimal weather conditions and constrained the VHE of the putative Swift-BAT source, achieving an upper-limit of 2.3×10^{-11} cm^{-2} s^{-1} above 0.5 TeV. We discussed two state-of-the-art physical mechanisms that could produce an observable VHE gamma-ray emission from a BBH merger embedded in the disk of an AGN:

1. The super-Eddington accretion onto a BBH system may produce observable EM signatures in proximity of the merger, however no considerations are made regarding the time delay with respect to the GW emission and the particle acceleration efficiency which may give rise to a VHE emission. Assuming a conversion factor of $\epsilon_\gamma = 0.1$, defined as the fraction of photons that are efficiently up-scattered up to VHE energies, we showed that, to be detected by our telescopes, a BBH merger similar to GW240615 and GW241125 should accrete with a super-Eddington efficiency of $\eta_{\rm bol} \geqslant 10^6$, which is several orders of magnitude above the known values of other super-Eddington accreting systems.
2. The shock breakout post-merger produced by the collision of a BZ jet with the dense gaseous disk of the AGN may give rise to thermal and non-thermal emission, on timescales that depend on the AGN properties, the localization of the BBH in the system and the distance of the event. The VHE emission is expected from inverse Compton scattering mechanism and it is highly dependent on the distance R of the merger from the central SMBH. A VHE signature from BBH events similar to GW240615 and GW241125 may be strong enough to be detected by MAGIC+LST-1 if $R \geqslant 1$, other than being more feasible for a follow-up by a ground-based telescope. However, we showed how, in the case of GW241125, the detection of a counterpart by Swift-BAT a few seconds after the GW rules out this possibility and indicates that the system was probably deeper inside the disk.

None of the mechanisms discussed above appears capable of producing a detectable VHE signal from GW240615 or GW241125. In addition, several challenges arise that are not directly related to the physical mechanisms behind such events: observing conditions, the time delay with respect to the GW signal, day–night constraints of our telescopes, and uncertainties regarding the true origin of the GWs. Nevertheless, our constraints suggest that a nearby event ($\leqslant$500 Mpc) could be detectable in the future, particularly given the expected increase in sensitivity with the full CTAO array (Cherenkov Telescope Array Consortium et al. 2019).

This work establishes a robust precedent for the VHE follow-up of GWs. Beyond the specific limits set on GW240615 and GW241125, the methodological frameworks developed here should serve as a base for future works treating sources with uncertain localization and sources observed in suboptimal weather conditions. Furthermore, our exploration of emission models extends the existing literature of GW counterparts observed with IACTs, preparing the necessary grounds for the upcoming CTAO.

Acknowledgments

A.S. gratefully acknowledges H. Tagawa for valuable discussions on theoretical aspects.

MAGIC collaboration acknowledgements: We would like to thank the Instituto de Astrofísica de Canarias for the excellent working conditions at the Observatorio del Roque de los Muchachos in La Palma. The financial support of the German BMFTR, MPG and HGF; the Italian INFN and INAF; the Swiss National Fund SNF; the grants PID2022-136828NB-C41, PID2022-137810NB-C22, PID2022-138172NB-C41, PID2022-138172NB-C42, PID2022-138172NB-C43, PID2022-139117NB-C41, PID2022-139117NB-C42, PID2022-139117NB-C43, PID2022-139117NB-C44, CNS2023-144504 funded by the Spanish MCIN/AEI/ 10.13039/501100011033 and "ERDF A way of making Europe"; the Indian Department of Atomic Energy; the Japanese ICRR, the University of Tokyo, JSPS, and MEXT; the Bulgarian Ministry of Education and Science, National RI Roadmap Project D01-135/16.07.2025 and the Academy of Finland grant No. 320045 is gratefully acknowledged. This work has also been supported by Centros de Excelencia "Severo Ochoa" y Unidades "María de Maeztu" program of the Spanish MCIN/ AEI/ 10.13039/501100011033 (CEX2019-000918-M, CEX2021-001131-S, CEX2024-001441-S), by AST22_00001_9 with funding from NextGenerationEU funds and by the CERCA institution and grants 2021SGR 00426, 2021SGR 00607 and 2021SGR 00773 of the Generalitat de Catalunya; by the Croatian Science Foundation (HrZZ) Project IP-2022-10-4595 and by the University of Rijeka Project uniri-mzi-25-3 funded by the European Union - NextGenerationEU; by the Deutsche Forschungsgemeinschaft (SFB1491) and by the Lamarr-Institute for Machine Learning and Artificial Intelligence; by the Polish Ministry of Science and Higher Education grant No. 2025/WK/04; by the European Union (ERC/MicroStars, 101076533 and INFRA/ACME, 101131928); and by the Brazilian MCTIC, the CNPq Productivity Grant 309053/2022-6 and FAPERJ Grants E-26/200.532/2023 and E-26/211.342/2021.

LST collaboration acknowledgements: We gratefully acknowledge financial support from the following agencies and organisations: Conselho Nacional de Desenvolvimento Científico e Tecnológico (CNPq) Grant 309053/2022-6 and Fundação de Amparo à Pesquisa do Estado do Rio de Janeiro (FAPERJ) Grants E-26/200.532/2023 and E-26/211.342/2021, Fundação de Amparo à Pesquisa do Estado de São Paulo (FAPESP), Fundação de Apoio à Ciência, Tecnologia e Inovação do Paraná—Fundação Araucária, Ministry of Science, Technology, Innovations and Communications (MCTIC), Brasil; the Bulgarian Ministry of Education and Science, National RI Roadmap Project D01-135/16.07.2025, Bulgaria; Croatian Science Foundation (HrZZ) Project IP-2022-10-4595; University of Rijeka Project uniri-mzi-25-3 funded by the European Union—NextGenerationEU; the following Croatian Institutions: Faculty of Physics, University of Rijeka; University Josip Juraj Strossmayer of Osijek; Faculty of Electrical Engineering, Mechanical Engineering and Naval Architecture (FESB), University of Split, Croatia; Ministry of Education, Youth and Sports, MEYS LM2023047, EU/MEYS CZ.02.1.01/0.0/0.0/16_013/0001403, CZ.02.1.01/0.0/0.0/18_046/0016007, CZ.02.1.01/0.0/0.0/16_019/0000754, CZ.02.01.01/00/22_008/0004632 and CZ.02.01.01/00/23_015/0008197 Czech Republic; CNRS-IN2P3, the French Programme d'investissements d'avenir and the Enigmass Labex, This work has been done thanks to the facilities offered by the Univ. Savoie Mont Blanc—CNRS/IN2P3 MUST computing center, France; Max Planck Society, German Bundesministerium für Forschung, Technologie und Raumfahrt (Verbundforschung / ErUM), the Deutsche Forschungsgemeinschaft (SFB 1491) and the Lamarr-Institute for Machine Learning and Artificial Intelligence, Germany; Istituto Nazionale di Astrofisica (INAF), Istituto Nazionale di Fisica Nucleare (INFN), Italian Ministry for University and Research (MUR), and the financial support from the European Union—Next Generation EU under the project IR0000012 - CTA+ (CUP C53C22000430006), announcement N.3264 on 28/12/2021: "Rafforzamento e creazione di IR nell'ambito del Piano Nazionale di Ripresa e Resilienza (PNRR)"; ICRR, University of Tokyo, JSPS, MEXT, Japan; JST SPRING—JPMJSP2108; Narodowe Centrum Nauki, grant number 2023/50/A/ST9/00254, Poland; The Spanish groups acknowledge the Spanish Ministry of Science and Innovation and the Spanish Research State Agency (AEI) through the government budget lines PGE2022/28.06.000X.711.04, 28.06.000X.411.01 and 28.06.000X.711.04 of PGE 2023, 2024 and 2025, and grants PID2019-104114RB-C31, PID2019-107847RB-C44, PID2019-105510GB-C31, PID2019-104114RB-C33, PID2019-107847RB-C43, PID2019-107847RB-C42, PID2019-107988GB-C22, PID2021-124581OB-I00, PID2021-125331NB-I00, PID2022-

136828NB-C41, PID2022-137810NB-C22, PID2022-138172NB-C41, PID2022-138172NB-C42, PID2022-138172NB-C43, PID2022-139117NB-C41, PID2022-139117NB-C42, PID2022-139117NB-C43, PID2022-139117NB-C44, PID2022-136828NB-C42, PID2024-155316NB-I00, PDC2023-145839-I00 funded by the Spanish MCIN/AEI/10.13039/501100011033 and by ERDF/EU and NextGenerationEU PRTR; CSIC PIE 202350E189; the "Centro de Excelencia Severo Ochoa" program through grants no. CEX2020-001007-S, CEX2021-001131-S, CEX2024-001441-S; the "Unidad de Excelencia María de Maeztu" program through grants no. CEX2019-000918-M, CEX2020-001058-M, CEX2024-001451-M; the "Ramón y Cajal" program through grants RYC2021-032991-I funded by MICIN/AEI/10.13039/501100011033 and the European Union "NextGenerationEU"/PRTR and RYC2020-028639-I; the "Juan de la Cierva-Incorporación" program through grant no. IJC2019-040315-I and "Juan de la Cierva-formación" through grant JDC2022-049705-I; the "'Viera y Clavijo" postdoctoral program of Universidad de La Laguna, funded by the Agencia Canaria de Investigación, Innovación y Sociedad de la Información. They also acknowledge the "Atracción de Talento" program of Comunidad de Madrid through grant no. 2019-T2/TIC-12900; "MAD4SPACE: Desarrollo de tecnologías habilitadoras para estudios del espacio en la Comunidad de Madrid" (TEC-2024/TEC-182) project, Doctorado Industrial (IND2024/TIC34250) and Ayudas para la contratación de personal investigador predoctoral en formación (PIPF-2023/TEC-29694) funded by Comunidad de Madrid; the La Caixa Banking Foundation, grant No. LCF/BQ/PI21/11830030; Junta de Andalucía under Plan Complementario de I+D+I (Ref. AST22_0001) and Plan Andaluz de Investigación, Desarrollo e Innovación as research group FQM-322; Project ref. AST22_00001_9 with funding from NextGenerationEU funds; the "Ministerio de Ciencia, Innovación y Universidades" and its "Plan de Recuperación, Transformación y Resiliencia"; "Consejería de Universidad, Investigación e Innovación" of the regional government of Andalucía and "Consejo Superior de Investigaciones Científicas," Grant CNS2023-144504 funded by MICIU/AEI/10.13039/501100011033 and by the European Union NextGenerationEU/PRTR, the European Union's Recovery and Resilience Facility-Next Generation, in the framework of the General Invitation of the Spanish Government's public business entity Red.es to participate in talent attraction and retention programmes within Investment 4 of Component 19 of the Recovery, Transformation and Resilience Plan; Junta de Andalucía under Plan Complementario de I+D+I (Ref. AST22_00001), Plan Andaluz de Investigación, Desarrollo e Innovación (Ref. FQM-322). "Programa Operativo de Crecimiento Inteligente" FEDER 2014-2020 (Ref. ESFRI-2017-IAC-12), Ministerio de Ciencia e Innovación, 15% co-financed by Consejería de Economía, Industria, Comercio y Conocimiento del Gobierno de Canarias; the "CERCA" program and the grants 2021SGR 00426 and 2021SGR 00679, all funded by the Generalitat de Catalunya; and the European Union's NextGenerationEU (PRTR-C17.I1). This work is funded/Co-funded by the European Union (ERC, MicroStars, 101076533). This research used the computing and storage resources provided by the Port d'Informació Científica (PIC) data center. State Secretariat for Education, Research and Innovation (SERI) and Swiss National Science Foundation (SNSF), Switzerland; The research leading to these results has received funding from the European Union's Seventh Framework Programme (FP7/2007-2013) under grant agreements No 262053 and No 317446; This project is receiving funding from the European Union's Horizon 2020 research and innovation programs under agreement No 676134; ESCAPE—The European Science Cluster of Astronomy & Particle Physics ESFRI Research Infrastructures has received funding from the European Union's Horizon 2020 research and innovation programme under Grant Agreement no. 824064.

A.S., P.G., J.S., A.S. acknowledge partial financial support by mobility "Canaletto" Program Italy-Poland 2025-2026 (MAECI: PL25MO12 and NAWA:BPN/BIT/2024/1/00037).

A.S. acknowledges financial support from INAF through the "Ricerca Fondamentale 2024" on the GO/GTO program titled "Discovering the New TeV Frontier of Gravitational Wave Counterparts through Follow-up Observations with the MAGIC Telescopes."

Facilities: MAGIC, CTAO LST-1.

Software: `gammapy v2.0` (Acero et al. 2025), `cta-lstchain v0.10.7` (Lopez-Coto et al. 2024), `MARS` (Zanin et al. 2013), `magic-cta-pipe` (Abe et al. 2023b), and packages therein.

Author Contribution

A. Simongini: project coordination, LST-1 and MAGIC data analysis, theoretical modelling, discussion and interpretation, paper drafting and editing. J. Jiménez Quiles: project coordination, main LST-1 and MAGIC data analysis, statistical methods, paper drafting and editing. M. Seglar Arroyo: project coordination, PI of the MAGIC+LST-1 proposal, AGN association analysis. M. Pecimotika: data analysis, paper drafting and editing. A. Moralejo: data analysis supervision and discussion A. Stamerra: PI of the MAGIC+LST-1 proposal, discussion. A. Carosi: discussion. S. Menon: fast offline analysis.

All authors above have participated in the paper discussion and edition. The rest of the authors have contributed in one or several of the following ways: design, construction, maintenance and operation of the instrument(s) used to acquire the data; preparation and/or evaluation of the observation proposals; data acquisition, processing, calibration and/or reduction; production of analysis tools and/or related Monte Carlo simulations; discussion and approval of the contents of the draft.

Appendix A
Addressing the NSB Conditions and Varying Energy Thresholds of Observations

A.1. GW240615

Observations of GW240615 were performed at relatively high zenith angles ranging 65 deg to 45 deg and after the Moon set on the horizon. In general, at large zenith angles the energy threshold can increase substantially, reaching values close to 1TeV in some cases (Aleksić et al. 2016; S. Abe et al. 2025). Additionally, LST-1 alone achieves an energy threshold about 2.5 times lower than that of MAGIC (López-Coto et al. 2021; Abe et al. 2023b), enabling access to gamma-rays at much lower energies. When combining data in stereo mode, requiring simultaneous observations with at least two telescopes, the resulting performance reflects the strengths of both configurations: MAGIC+LST-1 observations offer improved sensitivity at higher energies, while LST-1 alone provides better coverage in the low-energy range. We checked the totality of events distribution, composed mostly from hadronic background gamma-like events, as we need enough of these type to create a reliable background model (see Figure A1). In order to do that we find the median energy of the distributions run-wise, so we know where the bulk of the background statistics lies.

This complementarity makes it possible to tailor analyses to different energy domains and fully exploit the capabilities of the array. In particular, to get the best from our data, we performed two separate analyses: for the low-energy range between 0.15 TeV $< E_\gamma <$ 0.6 TeV we analysed LST-1 data alone, while for the high-energy range above $E_\gamma >$ 0.6 TeV we analysed MAGIC+LST-1 stereo data.

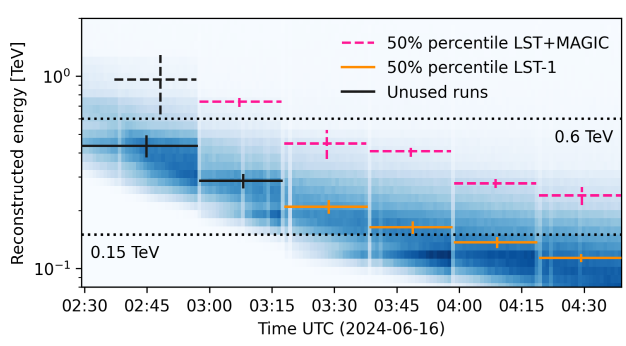

Figure A1. Run-wise median of the reconstructed event energy for GW240615, used to estimate energy threshold in the case of GW240615. The energy threshold is set in order to have enough background events to create a reliable background model. Horizontal lines separate the energy regions where the 50% of events are contained. Error bars represent the standard deviation of the percentile values, estimated over short time slices within each run. In the background histogram the total LST-1 distributions are shown in linear scale. The gaps results from changes of pointing and in some cases data removed because of the car flashes.

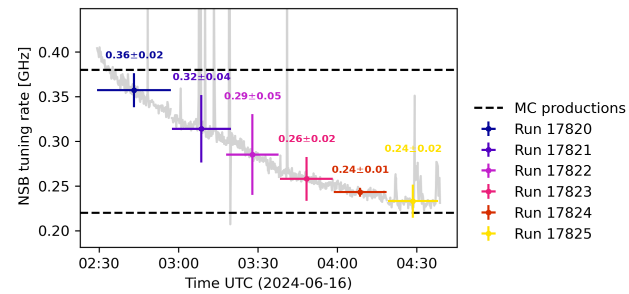

Figure A2. Variation of NSB level for images and waveforms for GW240615 observations with LST-1. The MC available productions are showed as dotted lines, and the sub-run wise values are plotted in gray in the background. The spikes that can be seen are produced by car-flashes, satellites or other light entering LST-1 camera.

Moreover, the observations are affected by a significantly varying NSB level. As shown in Figure A2, the NSB level decreased by approximately 45% over the course of two hours of observations, relative to the beginning of the run. These values are unusually high compared to typical extragalactic observations due to moonlight from the Moon being just below the horizon.

To account for these strong variations, Poisson noise is introduced into the simulated data. This can be either added at the waveform level (i.e., for each pixel signal, as implemented in `lstchain`) or at the image level (i.e., adding general noise to every pixel after the integration of signal, as implemented in `magic-cta-pipe`). We selected the most appropriate NSB tuning settings on a run-wise basis from the standard set of simulated values. For image-level noise, we considered NSB values of 2.0 and 2.5, expressed in units of the average number of photoelectrons per pixel. The NSB contribution was added as the standard deviation (square root) in the individual pixels. For waveform-level noise, the available levels used were 0.22 GHz and 0.38 GHz.

A.2. GW241125

For GW241125, we observed the source under suboptimal atmospheric conditions, including a cloud layer at ~6 km a.g.l. To illustrate the sky coverage achieved in these observations, we provide in Figure A3 the exposure map of GW241125. The map is obtained by summing the exposures across all reconstructed energy bins, and relatives 10th, 30th and 50th percentile thresholds are shown to highlight the regions with sufficient observational depth. This allows us to verify that the 95% localization region is fully observed. We represented the reconstructed energy distributions over the observations in Figure A4. The energy threshold seems to drop both for LST alone as for LST+MAGIC data, the general trend is given by the decrease of zenith angle. Given the exceptional suboptimal conditions the energy threshold is highly increased, and events at low energies contribute little due to their poor reconstruction

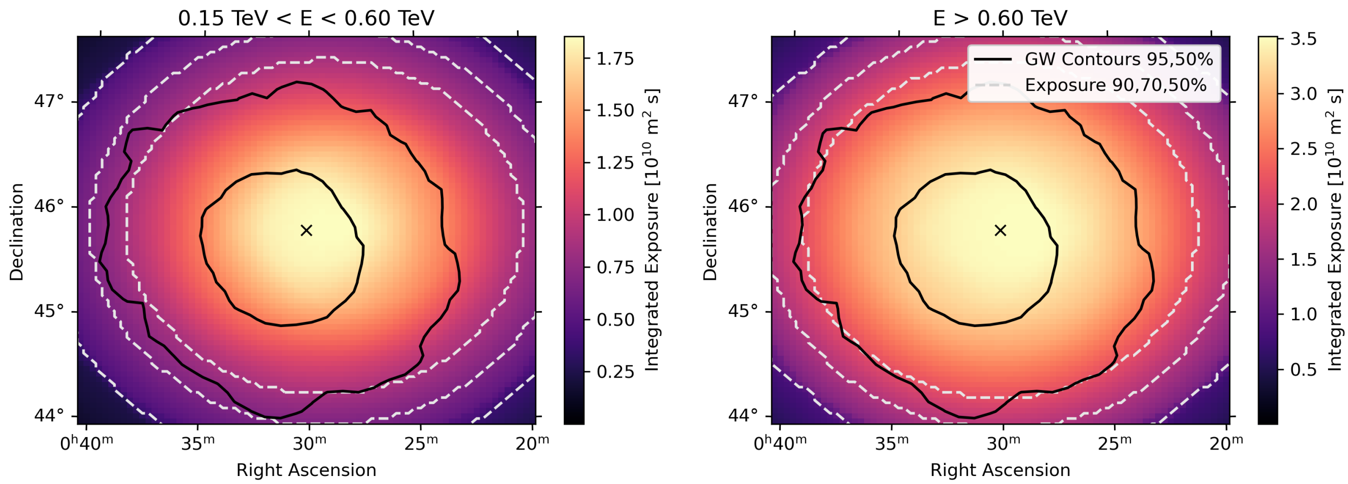

Figure A3. Integrated exposure of observations of GW241125. The exposure is computed for every energy bin of the analysis but here we integrated over all energy bins to get a unique exposure value of each bin. The contours of the 50% and 95% of the GW probability are shown as black solid lines. The 10th, 30th and 50th percentiles of the exposure are superposed in white dotted lines for each case.

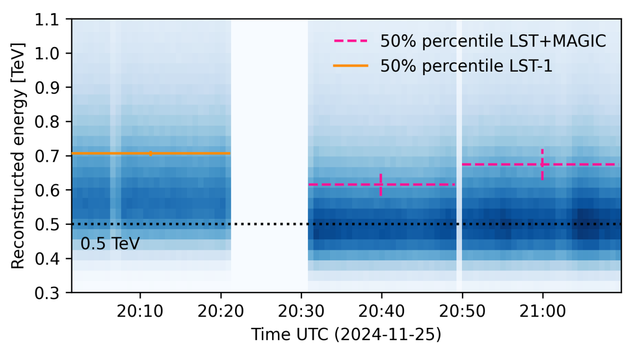

Figure A4. The run-wise median of the reconstructed event energy for GW241125 is represented in order to estimate energy threshold evolution. In the background, the total LST-1 event distributions are shown in linear scale. In orange, the LST-only runs used, in pink the LST+MAGIC runs used and in black the unused runs. The 50% percentile might not match with the peak of distributions in the background due to long tails toward larger energies.

quality. In order to go into a safe energy region, we analyse the data with reconstructed energy $E > 0.5$TeV.

Appendix B
Modifications to the Standard `gammapy` Analysis

The standard `gammapy v2.0` pipeline used for this analysis required two simple modifications in order to obtain meaningful upper limit sky-maps, as some needed options are not implemented in this version.

The class `ExcessMapEstimator` that is used to compute the sky-maps can yield negative flux values, and therefore, in some cases, the flux upper limit can be negative as well, leading to "non-physical" results. To ensure non-negative upper limits, in the pixels with negative excess, we set the number of observed counts equal to the background expectation, which will produce non-negative conservative upper limits. The limits are conservative in the sense that they will not "profit" from a deficit of events relative to the background expectation, lest it might be due to systematics, rather than just a background fluctuation.

The `ExcessMapEstimator` computes flux sky-maps by integrating counts within a correlation radius (see Section 5.2), but we are interested in the *total* flux from a point-like source instead. To obtain the needed conversion factor, a strong point-like source is simulated, using the same IRFs and analysis configuration as for the actual observation. The ratio between the injected flux and the average flux recovered within the correlation radius is the multiplicative factor needed to obtain the final flux upper limits on the bottom panels of Figure 3.

Appendix C
Results: Significance of Observations

C.1. Significance of GW240615

First we will discuss the significance of detection of the source GW240615. As the source location is not known, it is necessary to produce significance sky-maps, which were generated following the standard method described in first part of Section 5.2, with the resulting maps shown in Figure 3. No excess regions above the pre-trial 5σ threshold were detected.

We validated the background reconstruction using the projected distribution of pixel significances (Figure C1). This validation is done expecting no source in the field of view. In order to validate this we inspected all the background models in search of any inhomogeneity that can correspond to a source. We performed a Gaussian fit over the sky-maps and we get for the low-energies case $\mu = -0.07$ and $\sigma = 1.24$ while for high-energies $\mu = 0.08$ and $\sigma = 1.09$. In both energy

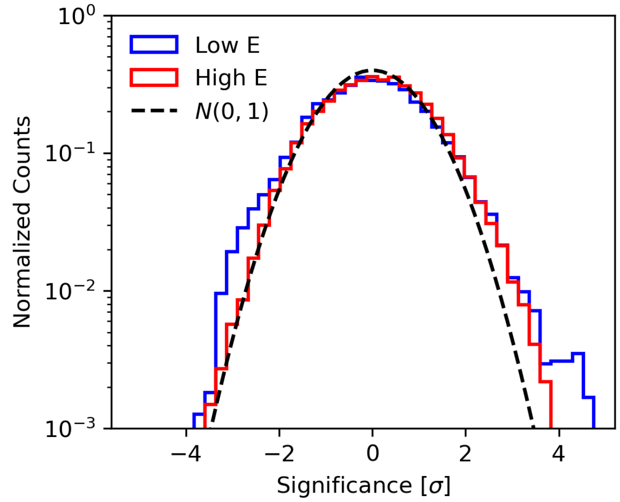

Figure C1. Projected distribution of significances for every pixel in the 95% interest region of the GW of the sky-map for GW240615, in different energy ranges. The ideal Gaussian ($\mu = 0$, $\sigma = 1$) is shown as a comparison.

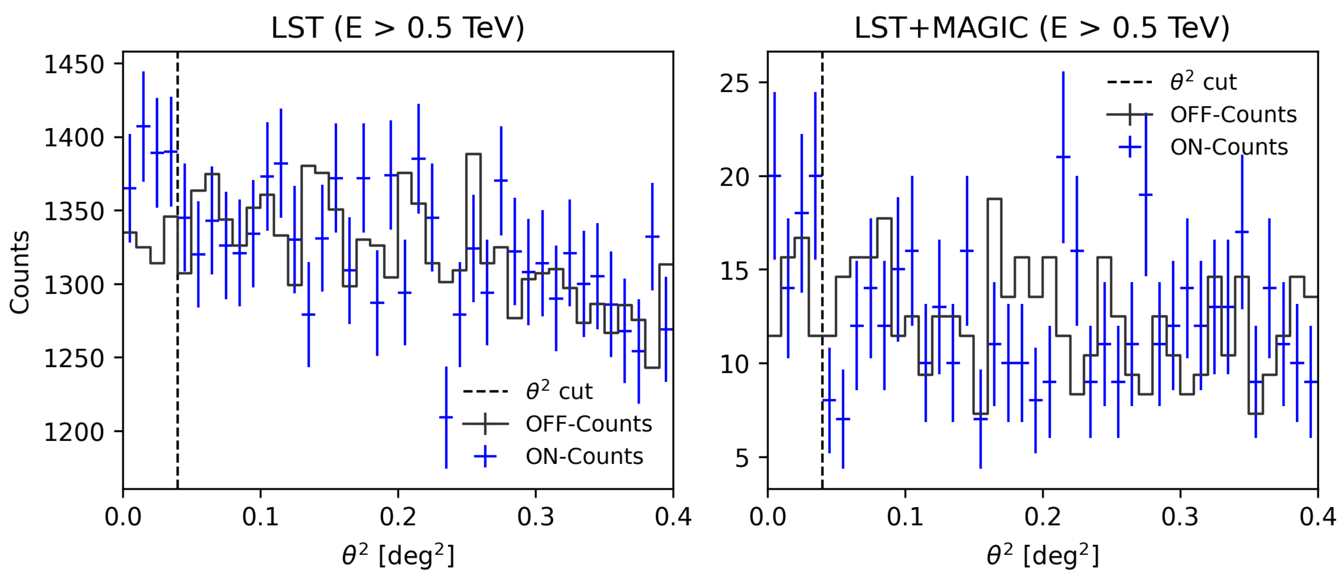

Figure C2. Distribution of squared angular distances of reconstructed events to the source position for GW241125. We show separately the LST-only run and the LST+MAGIC runs (where all events are stacked), and shown both for reconstructed energies $E > 0.5$ TeV. The obtained significances for both analysis are 2.2σ for LST-only and 1.47σ for LST+MAGIC data.

ranges, the Gaussian fit to the distribution closely follows a normal distribution with mean $\mu = 0$ and standard deviation $\sigma = 1$, as expected for a sky-map dominated by Poissonian noise fluctuations.

C.2. Significance of GW241125

We computed the significance of the source GW241125 using Li&Ma significance calculation Li & Ma (1983) based on the counts in the ON and OFF regions. We binned the data in quadratic angular (θ^2) bins so the area in the sky is constant for all bins. Then we set a θ cut of 0.2 deg to compute the number of events in both regions. Then we set 3 OFF regions symmetrically around the pointing position so the normalization factor $\alpha = 1/3$. Using Li&Ma significance formula we obtained a significance of 2.2σ for the LST data and 1.47σ for LST+MAGIC observations (see Figure C2).

ORCID iDs

S. Abe https://orcid.org/0000-0001-7250-3596
J. Abhir https://orcid.org/0000-0001-8215-4377
A. Abhishek https://orcid.org/0009-0005-5239-7905
V. A. Acciari https://orcid.org/0000-0001-8307-2007
F. Acero https://orcid.org/0000-0002-6606-2816
A. Aguasca-Cabot https://orcid.org/0000-0001-8816-4920
I. Agudo https://orcid.org/0000-0002-3777-6182
I. Albanese https://orcid.org/0009-0006-6223-5018
T. Aniello https://orcid.org/0009-0004-9368-0515
S. Ansoldi https://orcid.org/0000-0002-5613-7693
L. A. Antonelli https://orcid.org/0000-0002-5037-9034
C. Aramo https://orcid.org/0000-0002-8412-3846
A. Arbet-Engels https://orcid.org/0000-0001-9076-9582
C. Arcaro https://orcid.org/0000-0002-1998-9707
T.T.H. Arnesen https://orcid.org/0009-0004-0816-0700
A. Babić https://orcid.org/0000-0002-1444-5604
C. Bakshi https://orcid.org/0009-0007-1843-5386
A. Baktash https://orcid.org/0000-0002-5439-117X
A. Bamba https://orcid.org/0000-0003-0890-4920
A. Baquero Larriva https://orcid.org/0000-0002-1757-5826
U. Barres de Almeida https://orcid.org/0000-0001-7909-588X
J. A. Barrio https://orcid.org/0000-0002-0965-0259
L. Barrios Jiménez https://orcid.org/0009-0008-6006-175X
I. Batkovic https://orcid.org/0000-0002-1209-2542
J. Becerra González https://orcid.org/0000-0002-6729-9022
W. Bednarek https://orcid.org/0000-0003-0605-108X
E. Bernardini https://orcid.org/0000-0003-3108-1141
J. Bernete https://orcid.org/0000-0002-8108-7552
A. Berti https://orcid.org/0000-0003-0396-4190
C. Bigongiari https://orcid.org/0000-0003-3293-8522
A. Biland https://orcid.org/0000-0002-1288-833X
E. Bissaldi https://orcid.org/0000-0001-9935-8106
O. Blanch https://orcid.org/0000-0002-8380-1633
Ž. Bošnjak https://orcid.org/0000-0001-6536-0320
G. Bonnoli https://orcid.org/0000-0003-2464-9077
P. Bordas https://orcid.org/0000-0002-0266-8536
E. Bronzini https://orcid.org/0000-0001-8378-4303
G. Brunelli https://orcid.org/0009-0008-2078-2456
A. Bulgarelli https://orcid.org/0000-0001-6347-0649
I. Burelli https://orcid.org/0000-0002-8383-2202
A. Campoy-Ordaz https://orcid.org/0000-0001-9352-8936
M. Cardillo https://orcid.org/0000-0001-8877-3996
S. Caroff https://orcid.org/0000-0002-1103-130X
A. Carosi https://orcid.org/0000-0001-8690-6804
R. Carosi https://orcid.org/0000-0002-4137-4370
M. Carretero-Castrillo https://orcid.org/0000-0002-1426-1311
F. Cassol https://orcid.org/0000-0002-0372-1992
A. J. Castro-Tirado https://orcid.org/0000-0003-2999-3563
D. Cerasole https://orcid.org/0000-0003-2033-756X
G. Ceribella https://orcid.org/0000-0002-9768-2751
Y. Chai https://orcid.org/0000-0003-2816-2821
L. Chytka https://orcid.org/0000-0001-5741-259X
G. M. Cicciari https://orcid.org/0009-0007-3885-051X
A. Cifuentes Santos https://orcid.org/0000-0003-1033-5296
J. L. Contreras https://orcid.org/0000-0001-7282-2394
J. Cortina https://orcid.org/0000-0003-4576-0452
H. Costantini https://orcid.org/0000-0003-4027-3081
S. Covino https://orcid.org/0000-0001-9078-5507
P. Da Vela https://orcid.org/0000-0003-0604-4517
M. Dalchenko https://orcid.org/0000-0002-0137-136X
F. Dazzi https://orcid.org/0000-0001-5409-6544
A. De Angelis https://orcid.org/0000-0002-3288-2517
M. de Bony de Lavergne https://orcid.org/0000-0002-4650-1666
B. De Lotto https://orcid.org/0000-0003-3624-4480
R. de Menezes https://orcid.org/0000-0001-5489-4925
L. Del Peral https://orcid.org/0000-0003-2580-5668
M. Delfino https://orcid.org/0000-0002-9468-4751
C. Delgado Mendez https://orcid.org/0000-0002-7014-4101
J. Delgado Mengual https://orcid.org/0000-0002-0166-5464
D. della Volpe https://orcid.org/0000-0001-8530-7447
A. Di Piano https://orcid.org/0000-0002-9894-7491
F. Di Pierro https://orcid.org/0000-0003-4861-432X
R. Di Tria https://orcid.org/0009-0007-1088-5307
L. Di Venere https://orcid.org/0000-0003-0703-824X
C. Díaz https://orcid.org/0000-0002-5931-2709
D. Dominis Prester https://orcid.org/0000-0002-9880-5039
A. Donini https://orcid.org/0000-0002-3066-724X
D. Dorner https://orcid.org/0000-0001-8823-479X
M. Doro https://orcid.org/0000-0001-9104-3214
D. Elsässer https://orcid.org/0000-0001-6796-3205
G. Emery https://orcid.org/0000-0001-6155-4742
J. Escudero https://orcid.org/0000-0002-4131-655X
L. Fariña https://orcid.org/0000-0003-4116-6157
F. Ferrarotto https://orcid.org/0000-0001-5464-0378
A. Fiasson https://orcid.org/0000-0002-4209-6157
L. Foffano https://orcid.org/0000-0002-0709-9707
L. Font https://orcid.org/0000-0003-2109-5961
F. Frías García-Lago https://orcid.org/0009-0004-5848-8763
Y. Fukazawa https://orcid.org/0000-0002-0921-8837
R. J. García López https://orcid.org/0000-0002-8204-6832
D. Gasparrini https://orcid.org/0000-0002-5064-9495
S. Gasparyan https://orcid.org/0000-0002-0031-7759
M. Gaug https://orcid.org/0000-0001-8442-7877
N. Giglietto https://orcid.org/0000-0002-9021-2888
F. Giordano https://orcid.org/0000-0002-8651-2394
P. Gliwny https://orcid.org/0000-0002-4183-391X

N. Godinovic https://orcid.org/0000-0002-4674-9450
T. Gradetzke https://orcid.org/0000-0003-0646-2495
R. Grau https://orcid.org/0000-0002-1891-6290
J. Green https://orcid.org/0000-0002-1130-6692
S. Gunji https://orcid.org/0000-0002-5881-2445
P. Günther https://orcid.org/0009-0006-5372-440X
D. Hadasch https://orcid.org/0000-0001-8663-6461
A. Hahn https://orcid.org/0000-0003-0827-5642
T. Hassan https://orcid.org/0000-0002-4758-9196
K. Hayashi https://orcid.org/0000-0002-8758-8139
L. Heckmann https://orcid.org/0000-0002-6653-8407
M. Heller https://orcid.org/0000-0003-1215-0148
J. Herrera Llorente https://orcid.org/0000-0002-3771-4918
D. Hoffmann https://orcid.org/0000-0001-5209-5265
D. Horns https://orcid.org/0000-0003-1945-0119
J. Houles https://orcid.org/0000-0002-5373-7992
D. Hrupec https://orcid.org/0000-0002-7027-5021
T. Inada https://orcid.org/0000-0002-6923-9314
S. Inoue https://orcid.org/0000-0003-1096-9424
K. Ioka https://orcid.org/0000-0002-3517-1956
M. Iori https://orcid.org/0000-0002-6349-0380
D. Israyelyan https://orcid.org/0000-0002-5804-6605
A. Iuliano https://orcid.org/0000-0001-6087-9633
I. Jiménez Martínez https://orcid.org/0000-0003-2150-6919
J. Jiménez Quiles https://orcid.org/0009-0005-6729-5709
J. Jurysek https://orcid.org/0000-0002-3130-4168
V. Karas https://orcid.org/0000-0002-5760-0459
H. Katagiri https://orcid.org/0000-0003-2347-8819
T. Kayanoki https://orcid.org/0000-0002-6960-9274
D. Kerszberg https://orcid.org/0000-0002-5289-1509
G. W. Kluge https://orcid.org/0009-0009-0384-0084
Y. Kobayashi https://orcid.org/0009-0005-5680-6614
K. Kohri https://orcid.org/0000-0003-3764-8612
P. M. Kouch https://orcid.org/0000-0002-9328-2750
H. Kubo https://orcid.org/0000-0001-9159-9853
J. Kushida https://orcid.org/0000-0002-8002-8585
M. Láinez https://orcid.org/0000-0003-3848-922X
A. Lamastra https://orcid.org/0000-0003-2403-913X
E. Lindfors https://orcid.org/0000-0002-9155-6199
M. Linhoff https://orcid.org/0000-0001-7993-8189
F. Longo https://orcid.org/0000-0003-2501-2270
R. López-Coto https://orcid.org/0000-0002-3882-9477
M. López-Moya https://orcid.org/0000-0002-8791-7908
A. López-Oramas https://orcid.org/0000-0003-4603-1884
S. Loporchio https://orcid.org/0000-0003-4457-5431
P. L. Luque-Escamilla https://orcid.org/0000-0002-3306-9456
P. Majumdar https://orcid.org/0000-0002-5481-5040
M. Makariev https://orcid.org/0000-0002-1622-3116
M. Mallamaci https://orcid.org/0000-0003-4068-0496
D. Mandat https://orcid.org/0000-0001-7748-7468
G. Maneva https://orcid.org/0000-0002-5959-4179
M. Manganaro https://orcid.org/0000-0003-1530-3031
S. Mangano https://orcid.org/0000-0001-5872-1191
K. Mannheim https://orcid.org/0000-0002-2950-6641
M. Mariotti https://orcid.org/0000-0003-3297-4128
G. Marsella https://orcid.org/0000-0002-3152-8874
J. Martí https://orcid.org/0000-0001-5302-0660
G. Martínez https://orcid.org/0000-0002-1061-8520
M. Martínez https://orcid.org/0000-0002-9763-9155
O. Martinez https://orcid.org/0000-0002-3353-7707
P. Maruševec https://orcid.org/0000-0002-6748-4615
D. Mazin https://orcid.org/0000-0002-2010-4005
J. Méndez-Gallego https://orcid.org/0009-0006-6222-5813
E. Mestre Guillen https://orcid.org/0000-0003-3968-1782
D. Miceli https://orcid.org/0000-0002-2686-0098
T. Miener https://orcid.org/0000-0003-1821-7964
J. M. Miranda https://orcid.org/0000-0002-1472-9690
R. Mirzoyan https://orcid.org/0000-0003-0163-7233
M. Molero Gonzalez https://orcid.org/0000-0003-0967-715X
E. Molina https://orcid.org/0000-0003-1204-5516
H. A. Mondal https://orcid.org/0000-0001-7217-0234
T. Montaruli https://orcid.org/0000-0001-5014-2152
A. Moralejo https://orcid.org/0000-0002-1344-9080
A. Morselli https://orcid.org/0000-0002-7704-9553
V. Moya https://orcid.org/0000-0001-9407-5545
A. L. Müller https://orcid.org/0000-0002-8473-695X
H. Muraishi https://orcid.org/0000-0003-3054-5725
T. Nakamori https://orcid.org/0000-0002-7308-2356
C. Nanci https://orcid.org/0000-0002-1791-8235
V. Neustroev https://orcid.org/0000-0003-4772-595X
M. Nievas Rosillo https://orcid.org/0000-0002-8321-9168
C. Nigro https://orcid.org/0000-0001-8375-1907
K. Noda https://orcid.org/0000-0003-1397-6478
V. Novotny https://orcid.org/0000-0002-4319-4541
S. Nozaki https://orcid.org/0000-0002-6246-2767
M. Ohishi https://orcid.org/0000-0002-5056-0968
A. Okumura https://orcid.org/0000-0002-3055-7964
J. Otero- Santos https://orcid.org/0000-0002-4241-5875
P. Ottanelli https://orcid.org/0000-0001-6506-6674
S. Paiano https://orcid.org/0000-0002-2239-3373
M. Palatiello https://orcid.org/0000-0002-4124-5747
G. Panebianco https://orcid.org/0000-0002-3410-8613
D. Paneque https://orcid.org/0000-0002-2830-0502
R. Paoletti https://orcid.org/0000-0003-0158-2826
J. M. Paredes https://orcid.org/0000-0002-1566-9044
M. Pech https://orcid.org/0000-0002-8421-0456
M. Pecimotika https://orcid.org/0000-0002-4699-1845
M. Peresano https://orcid.org/0000-0002-7537-7334
F. Perrotta https://orcid.org/0000-0002-5930-3669
M. Persic https://orcid.org/0000-0003-1853-4900
M. Pihet https://orcid.org/0009-0000-4691-3866
G. Pirola https://orcid.org/0000-0002-2507-2612
C. Plard https://orcid.org/0000-0002-4061-3800

F. Podobnik https://orcid.org/0000-0001-6125-9487
P. G. Prada Moroni https://orcid.org/0000-0001-9712-9916
E. Prandini https://orcid.org/0000-0003-4502-9053
S. Rainò https://orcid.org/0000-0002-9181-0345
R. Rando https://orcid.org/0000-0001-6992-818X
W. Rhode https://orcid.org/0000-0003-2636-5000
M. Ribó https://orcid.org/0000-0002-9931-4557
J. Rico https://orcid.org/0000-0003-4137-1134
G. Rodriguez Fernandez https://orcid.org/0000-0002-4683-230X
E. Ruiz-Velasco https://orcid.org/0000-0001-6939-7825
N. Sahakyan https://orcid.org/0000-0003-2011-2731
T. Saito https://orcid.org/0000-0001-6201-3761
S. Sakurai https://orcid.org/0000-0001-7427-4520
D. A. Sanchez https://orcid.org/0000-0002-7210-4496
H. Sano https://orcid.org/0000-0003-2062-5692
T. Šaric https://orcid.org/0000-0001-8731-8369
Y. Sato https://orcid.org/0000-0003-2477-9146
F. G. Saturni https://orcid.org/0000-0002-1946-7706
V. Savchenko https://orcid.org/0000-0001-6353-0808
K. Schmitz https://orcid.org/0000-0002-9883-4454
F. Schussler https://orcid.org/0000-0003-1500-6571
M. Seglar Arroyo https://orcid.org/0000-0001-8654-409X
A. Simongini https://orcid.org/0009-0000-3416-9865
J. Sitarek https://orcid.org/0000-0002-1659-5374
V. Sliusar https://orcid.org/0000-0002-4387-9372
D. Sobczynska https://orcid.org/0000-0003-4973-7903
A. Stamerra https://orcid.org/0000-0002-9430-5264
J. Striškovic https://orcid.org/0000-0003-2902-5044
D. Strom https://orcid.org/0000-0003-2108-3311
M. Strzys https://orcid.org/0000-0001-5049-1045
Y. Suda https://orcid.org/0000-0002-2692-5891
A. Sunny https://orcid.org/0009-0002-2493-8987
H. Tajima https://orcid.org/0000-0002-1721-7252
M. Takahashi https://orcid.org/0000-0002-0574-6018
R. Takeishi https://orcid.org/0000-0001-6335-5317
S. J. Tanaka https://orcid.org/0000-0002-8796-1992
P. Temnikov https://orcid.org/0000-0002-9559-3384
Y. Terada https://orcid.org/0000-0002-2359-1857
K. Terauchi https://orcid.org/0009-0002-3519-2535
T. Terzic https://orcid.org/0000-0002-4209-3407
D. F. Torres https://orcid.org/0000-0002-1522-9065
P. Travnicek https://orcid.org/0000-0002-1655-9584
A. Tutone https://orcid.org/0000-0002-2840-0001
S. Ubach https://orcid.org/0000-0002-6159-5883
M. Vacula https://orcid.org/0000-0003-4844-3962
M. Vázquez Acosta https://orcid.org/0000-0002-2409-9792
G. Verna https://orcid.org/0000-0001-5916-9028
I. Viale https://orcid.org/0000-0001-5031-5930
A. Vigliano https://orcid.org/0009-0001-3508-4019
C. F. Vigorito https://orcid.org/0000-0002-0069-9195
E. Visentin https://orcid.org/0000-0002-8497-5985
V. Vitale https://orcid.org/0000-0001-8040-7852
G. Voutsinas https://orcid.org/0009-0007-9386-5810
I. Vovk https://orcid.org/0000-0003-3444-3830
T. Vuillaume https://orcid.org/0000-0002-5686-2078
R. Walter https://orcid.org/0000-0003-2362-4433
F. Wersig https://orcid.org/0009-0006-1828-6117
R. Yamazaki https://orcid.org/0000-0002-1251-7889
T. Yoshida https://orcid.org/0000-0002-7708-6362
T. Yoshikoshi https://orcid.org/0000-0002-6045-9839
W. Zhang https://orcid.org/0000-0003-2839-1325

References

Aasi, J., Abbott, B., Abbott, R., et al. 2015, CQGra, 32, 074001
Abac, A. G., Abbott, R., Abouelfettouh, I., et al. 2024, ApJL, 970, L34
Abac, A. G., Abouelfettouh, I, Acernese, F, et al. 2025, ApJL, 993, L25
Abbasi, R., Ackermann, M., Adams, J., et al. 2023, ApJ, 944, 80
Abbott, B., Abbott, R., Abbott, T., et al. 2019, PhRvX, 9, 011001
Abbott, B. P., Abbott, R., Abbott, T. D., et al. 2016, PhRvL, 116, 061102
Abbott, B. P., Abbott, R., Abbott, T., et al. 2017a, PhRvL, 119, 161101
Abbott, B. P., Abbott, R., Abbott, T., et al. 2017b, ApJL, 848, L13
Abbott, B. P., Abbott, R., Abbott, T. D., et al. 2017, ApJL, 848, L12
Abbott, B. P., Abbott, R., Abbott, T., et al. 2019a, PhRvX, 9, 031040
Abbott, B. P., Abbott, R., Abbott, T., et al. 2019b, PhRvL, 123, 011102
Abbott, B. P., Abbott, R., Abbott, T., et al. 2020, ApJ, 892, L3
Abbott, R., Abbott, T., Abraham, S., et al. 2021a, PhRvX, 11, 021053
Abbott, R., Abbott, T. D., Abraham, S., et al. 2021b, ApJL, 915, L5
Abbott, R., Abbott, T., Acernese, F., et al. 2023, PhRvX, 13, 041039
Abbott, R., Abbott, T., Acernese, F., et al. 2024, PhRvD, 109, 022001
Abdalla, H., Abramowski, A., Aharonian, F., et al. 2017, ApJL, 850, L22
Abdalla, H., Adam, R., Aharonian, F., et al. 2020, ApJL, 894, L16
Abdalla, H., Aharonian, F., Benkhali, F. A., et al. 2021, ApJ, 923, 109
Abdollahi, S., Acero, F., Ackermann, M., et al. 2020, ApJS, 247, 33
Abe, H., Abe, K., Abe, S., et al. 2023a, ApJ, 956, 80
Abe, H., Abe, K., Abe, S., et al. 2023b, A&A, 680, A66
Abe, S., Abhishek, Doro, M., et al. 2025, EPJWC, 319, 05006
Abramowicz, M. A., & Fragile, P. C. 2013, LRR, 16, 1
Acciari, V. A., Ansoldi, S., Antonelli, L. A., et al. 2021, ApJ, 908, 90
Acernese, F., Agathos, M., Agatsuma, K., et al. 2014, CQGra, 32, 024001
Acero, F., Aguasca-Cabot, A., Barrios-Jiménez, L., et al. 2025, Gammapy: Python toolbox for gamma-ray astronomy, v2.0, Zenodo, doi: 10.5281/zenodo.17814297
Akl, D., Masek, M., Andrade, C., et al. 2024a, GCN, 36705, 1
Akl, D., Andrade, C., de Bruin, E., et al. 2024b, GCN, 38396, 1
Aleksić, J., Ansoldi, S., Antonelli, L. A., et al. 2015, JHEAp, 5, 30
Aleksić, J., Ansoldi, S., Antonelli, L. A., et al. 2016, APh, 72, 76
Aso, Y., Michimura, Y., Somiya, K., et al. 2013, PhRvD, 88, 043007
Bahcall, J. N., & Wolf, R. A. 1976, ApJ, 209, 214
Bambi, C., & Santangelo, A. 2024, Handbook of X-Ray and Gamma-Ray Astrophysics (Springer Nature)
Baret, B., Bartos, I., Bouhou, B., et al. 2012, PhRvD, 85, 103004
Bartos, I., Brady, P., & Marka, S. 2013a, CQGra, 30, 123001
Bartos, I., Haiman, Z., Kocsis, B., & Márka, S. 2013b, PhysRevLett, 110, 221102
Bartos, I., Haiman, Z., Marka, Z., et al. 2017a, NatCo, 8, 831
Bartos, I., Kocsis, B., Haiman, Z., & Márka, S. 2017b, ApJ, 835, 165
Bartos, I., Veske, D. b. u., Keivani, A., et al. 2019, PhRvD, 100, 083017
Becerra, R. L., Troja, E., Angulo Valdez, C., et al. 2024, GCN, 38329, 1
Begelman, M. C. 2002, ApJ, 568, L97
Belloni, T. M., & Motta, S. E. 2016, ASSL, 440, 61
Berge, D., Funk, S., & Hinton, J. 2007, A&A, 466, 1219
Berk, A., Bernstein, L., & Robertson, D. 1987, MODTRAN: A moderate resolution model for LOWTRAN, SSI-TR-124, SCIENTIFIC-1, Spectral Sciences, Inc., Burlington, MA Technical rept. 12 May 1986-11 May 1987
Bernlöhr, K. 2000, APh, 12, 255
Bernlöhr, K. 2008, APh, 30, 149

Blandford, R. D., & Znajek, R. L. 1977, MNRAS, 179, 433
Carosi, A., Ashkar, H., Berti, A., et al. 2021, ICRC, 395, 838
Chen, T. W., Brennan, S. J., Ronchini, S., et al. 2024, GCN, 38314, 1
Cherenkov Telescope Array Consortium, Acharya, B. S., Agudo, I., et al. 2019, Science with the Cherenkov Telescope Array (World Scientific Publishing Co. Pte. Ltd.)
Connaughton, V., Burns, E., Goldstein, A., et al. 2016, ApJL, 826, L6
Connaughton, V., Burns, E., Goldstein, A., et al. 2018, ApJL, 853, L9
DeLaunay, J., Tohuvavohu, A., Ronchini, S., et al. 2024a, GCN, 38308, 1
DeLaunay, J., Tohuvavohu, A., Ronchini, S., et al. 2024b, GCN, 38351, 1
Donath, A., Terrier, R., Remy, Q., et al. 2023, A&A, 678, A157
Duffell, P. C. 2015, ApJL, 807, L11
Dálya, G., Díaz, R., Bouchet, F. R., et al. 2022, MNRAS, 514, 1403
Evans, P., Kennea, J., Palmer, D., et al. 2016, MNRAS, 462, 1591
Evans, P. A., Page, K. L., Kennea, J. A., et al. 2024, GCN, 36837, 1
Farrell, S. A., Webb, N. A., Barret, D., Godet, O., & Rodrigues, J. M. 2009, Natur, 460, 73
Farris, B. D., Liu, Y. T., & Shapiro, S. L. 2010, PhysRevD, 81, 084008
Flaminio, R. 2020, SPIE, 11445, 1144511
Flesch, E. W. 2016, PASA, 33, e052
Flesch, E. W. 2023, OJAp, 6, 49
Fomin, V., Stepanian, A., Lamb, R., et al. 1994, APh, 2, 137
Ford, K. S., & McKernan, B. 2022, MNRAS, 517, 5827
Fruck, C., Gaug, M., Hahn, A., et al. 2022, MNRAS, 515, 4520
Fu, Q. 1996, JCli, 9, 2058
Gaia Collaboration, Bailer-Jones, C. A. L., Teyssier, D., et al. 2023, A&A, 674, A41
Gerosa, D., & Fishbach, M. 2021, NatAs, 5, 749
Ghosh, S., Bloemen, S., Nelemans, G., Groot, P. J., & Price, L. R. 2016, A&A, 592, A82
Goldstein, A., Veres, P., Burns, E., et al. 2017, ApJL, 848, L14
Graham, M., Ford, K., McKernan, B., et al. 2020, PhRvL, 124, 251102
Greene, J. E., & Ho, L. C. 2009, ApJ, 704, 1743
Greisen, E. G., Valdes, F. G., Calabretta, M. R., & Allen, S. L. 2003, ASPC, 295, 403
Górski, K. M., Hivon, E., Banday, A. J., et al. 2005, ApJ, 622, 759
Hailey, C. J., Mori, K., Bauer, F. E., et al. 2018, Natur, 556, 70
Hearn, D. 1969, NucIM, 70, 200
Heck, D., Knapp, J., Capdevielle, J. N., et al. 1998, CORSIKA: A Monte Carlo code to simulate extensive air showers, Report fzka (Report fzka) 6019
Hillas, A. M. 1985, ICRC, 3, 445
Hirata, K., Kajita, T., Koshiba, M., et al. 1988, PhRvD, 38, 448
Hussain, R., Vandenbroucke, J., & Wood, J. 2020, ICRC, 358, 918
Jiang, S. Q., Liu, X., Fu, S. Y., et al. 2024, GCN, 38328, 1
Jiang, Y.-F., Stone, J. M., & Davis, S. W. 2014, ApJ, 796, 106
Kimura, S. S., Murase, K., & Bartos, I. 2021, ApJ, 916, 111
Klingler, N. J., Oates, S. R., Tohuvavohu, A., et al. 2024, GCN, 38350, 1
Kocevski, D., Omodei, N., Buson, S., et al. 2017, GCN, 21534, 1
Kohnle, A., Aharonian, F., Akhperjanian, A., et al. 1996, APh, 5, 119
Li, T., Xiong, S., Zhang, S., et al. 2018, SCPMA, 61, 1
Li, T. P., & Ma, Y. Q. 1983, ApJ, 272, 317
Lopez-Coto, R., Vuillaume, T., Moralejo, A., et al. 2024, cta-observatory/cta-lstchain: v0.10.7 - 2024-02-01, Zenodo, doi: 10.5281/zenodo.10604579
LVK Collaboration 2024a, GCN, 36669, 1
LVK Collaboration 2024b, GCN, 36704, 1
LVK Collaboration 2024c, GCN, 38305, 1
LVK Collaboration 2024d, GCN, 38313, 1
LVK Collaboration 2026a, arXiv:2605.27225
LVK Collaboration 2026b, arXiv:2605.27226
López-Coto, R., Moralejo, A., Artero, M., et al. 2021, ICRC, 395, 806
Martinez-Castellanos, I., Smith, A., Collaboration, H., et al. 2017, GCN, 21683, 1
McKernan, B., Ford, K., Bartos, I., et al. 2019, ApJL, 884, L50
McKinney, J. C., Tchekhovskoy, A., Sadowski, A., & Narayan, R. 2014, MNRAS, 441, 3177
Miceli, D., Antonelli, L. A., Gonzalez, J. B., et al. 2019, ICRC, 358, 743
Mohan, T., Waratkar, G., Saikia, A. P., et al. 2024, GCN, 38325, 1
Moralejo, A., Gaug, M., Carmona, E., et al. 2009, MARS: The MAGIC Analysis and Reconstruction Software, ascl:1011.004
Morris, M. 1993, ApJ, 408, 496
Murase, K., Kashiyama, K., Mészáros, P., Shoemaker, I., & Senno, N. 2016, ApJL, 822, L9
Nakahira, S., Yoshida, A., Sakamoto, T., et al. 2017, GCN, 21641, 1
Noethe, M., Kosack, K., Nickel, L., Peresano, M., & Consortium, C. 2022, ICRC, 37, 744
O'Leary, R. M., Kocsis, B., & Loeb, A. 2009, MNRAS, 395, 2127
Page, K. L., Evans, P. A., Kennea, J. A., et al. 2024a, GCN, 36698, 1
Page, K. L., Evans, P. A., Kennea, J. A., et al. 2024b, GCN, 38324, 1
Pecimotika, M., Dominis Prester, D., Hrupec, D., et al. 2023, JCAP, 2023, 011
Pinto, C., & Walton, D. J. 2023, in High-Resolution X-ray Spectroscopy: Instrumentation, Data Analysis, and Science (Springer), 345
Planck Collaboration, Aghanim, N., Akrami, Y., et al. 2020, A&A, 641, A6
Rastinejad, J. C., Shrestha, M., Hosseinzadeh, G., et al. 2024, GCN, 38333, 1
Reguitti, A., Tartaglia, L., Tomasella, L., et al. 2024, GCN, 36972, 1
Ridnaia, A., Frederiks, D., Lysenko, A., et al. 2024, GCN, 38321, 1
Ronchini, S., Tohuvavohu, A., Kennea, J. A., et al. 2024, GCN, 36687, 1
Santander, M. 2019, ICRC, 36, 782
Savchenko, V., Ferrigno, C., Rodi, J., et al. 2024, GCN, 38311, 1
Savchenko, V., Ferrigno, C., Kuulkers, E., et al. 2017, ApJL, 848, L15
Schlafly, E. F., Meisner, A. M., & Green, G. M. 2019, ApJS, 240, 30
Schmuckermaier, F., Gaug, M., Fruck, C., et al. 2023, A&A, 673, A2
Scotton, L. & Fermi-GBM Team 2024, GCN, 38316, 1
Seglar-Arroyo, M., Ashkar, H., de Lavergne, M. d. B., & Schüssler, F. 2024, ApJS, 274, 1
Seglar-Arroyo, M., Berti, A. A., Carosi, G. M. C., et al. 2025, in 39th Int. Cosmic Ray Conf. (ICRC2025), 501, (PoS)
Serrano, D., Marín, M. J., Núñez, M., et al. 2015, JASTP, 130, 14
Shakura, N. I., & Sunyaev, R. A. 1973, A&A, 24, 337
Sobczynska, D., & Bednarek, W. 2014, JPhG, 41, 125201
Stamerra, A., Salafia, O. S., Berti, A., et al. 2022, ICRC, 395, 944
Stone, N. C., Metzger, B. D., & Haiman, Z. 2017, MNRAS, 464, 946
Storey-Fisher, K., Hogg, D. W., Rix, H.-W., et al. 2024, ApJ, 964, 69
Strzys, M. C., et al. 2023, ICRC, 444, 894
Svinkin, D., Golenetskii, S., Aptekar, R., et al. 2017, GCN, 21746, 1
Swain, V., Teja, R. S., Mohan, T., et al. 2024, GCN, 38322, 1
Tagawa, H., Haiman, Z., & Kocsis, B. 2020, ApJ, 898, 25
Tagawa, H., Kimura, S. S., & Haiman, Z. 2023, ApJ, 955, 23
Tagawa, H., Kimura, S. S., Haiman, Z., Perna, R., & Bartos, I. 2023, ApJ, 950, 13
Tagawa, H., Kimura, S. S., Haiman, Z., Perna, R., & Bartos, I. 2024, ApJ, 966, 21
Tagawa, H., Kimura, S. S., Haiman, Z., et al. 2022, ApJ, 927, 41
Verrecchia, F., Tavani, M., Donnarumma, I., et al. 2017, ApJL, 850, L27
Veske, D., Márka, Z., Bartos, I., & Márka, S. 2020, JCAP, 2020, 016
Vianello, G., Omodei, N., Chiang, J., & Digel, S. 2017, ApJL, 841, L16
Wang, Y. L., Wen, S. X., Wang, W. X., et al. 2024, GCN, 38345, 1
Watson, A. M., Antier, S., Basa, S., et al. 2024, GCN, 38317, 1
Woosley, S., & Heger, A. 2021, ApJL, 912, L31
Xue, L., Tagawa, H., Haiman, Z., & Bartos, I. 2025, PhysRevD, 112, 063034
Yang, Y., Bartos, I., Gayathri, V., et al. 2019, PhRvL, 123, 181101
Zanin, R., Carmona, E., Sitarek, J., et al. 2013, ICRC, 33, 2937
Zhang, S.-R., Wang, Y., Yuan, Y.-F., et al. 2026, ApJ, 998, 171
Żywucka, N., Sitarek, J., Sobczyńska, D., et al. 2024, A&A, 685, A165